THE GEOLOGICAL SOCIETY OF AMERICA®

BULLETIN

E: gsab@geosociety.org
W: geosociety.org/gsa
T: @geosociety

Travertine records climate-induced transformations of the Yellowstone hydrothermal system from the late Pleistocene to the Present

Tracking no: B37317R

Authors:
Lauren Harrison (Colorado State University), Shaul Hurwitz (US Geological Survey), James Paces (U.S. Geological Survey), Cathy Whitlock (Montana State University), Sara Peek (US Geological Survey), and Joseph Licciardi (University of New Hampshire)

Abstract:
Chemical changes in hot springs, as recorded by thermal waters and their deposits, provide a window into the evolution of the postglacial hydrothermal system of the Yellowstone Plateau Volcanic Field. Today, most hydrothermal travertine forms to the north and south of the 631-ka Yellowstone caldera where groundwater flow through subsurface sedimentary rocks allows for calcite saturation at hot springs. In contrast, low-Ca rhyolites dominate the subsurface within the Yellowstone caldera, resulting in thermal waters that rarely deposit travertine. We investigate the timing and origin of five small travertine deposits in the Upper and Lower Geyser Basins to understand the conditions that allowed for travertine deposition. New 230Th-U dating, oxygen (δ18O), carbon (δ13C), and strontium (87Sr/86Sr) isotopic values, and elemental concentrations indicate that travertine deposits within the Yellowstone caldera formed during three main episodes that correspond broadly with known periods of wet climate: 13.9-13.6 ka, 12.2-9.5 ka, and 5.2-2.9 ka. Travertine deposition was in response to the influx of large volumes of cold meteoric water that increased the rate of chemical weathering of surficial sediments and recharge into the hydrothermal system. The small volume of intra-caldera travertine does not support a massive postglacial surge of CO2 within the Yellowstone caldera nor is magmatic CO2 the catalyst for postglacial travertine deposition.

Travertine records climate-induced transformations of the Yellowstone hydrothermal system from the late Pleistocene to the Present

Lauren N. Harrison[1,2], Shaul Hurwitz[2], James B. Paces[3], Cathy Whitlock[4], Sara Peek[2], Joseph Licciardi[5]

[1]*Department of Geosciences, Colorado State University, 1482 Campus Delivery, Fort Collins, CO, 80523-1482, USA*

[2]*U.S. Geological Survey, Volcano Science Center, 350 N. Akron Rd, Moffett Field, CA, 94035, USA*

[3]*U.S. Geological Survey, Denver Federal Center, P.O. Box 25046, MS 980, Lakewood, CO, 80225, USA*

[4] *Department of Earth Sciences, Montana State University, Leon Johnson Hall 710, Bozeman, MT, 59715, USA*

[5] *Department of Earth Sciences, University of New Hampshire, James Hall Room 316, Durham, NH, 03824, USA*

ABSTRACT

Chemical changes in hot springs, as recorded by thermal waters and their deposits, provide a window into the evolution of the postglacial hydrothermal system of the Yellowstone Plateau Volcanic Field. Today, most hydrothermal travertine forms to the north and south of the 631-ka Yellowstone caldera where groundwater flow through subsurface sedimentary rocks allows for calcite saturation at hot springs. In contrast, low-Ca rhyolites dominate the subsurface within the Yellowstone caldera, resulting in thermal waters that rarely deposit travertine. We investigate the timing and origin of five small travertine deposits in the Upper and Lower Geyser

Basins to understand the conditions that allowed for travertine deposition. New ^{230}Th-U dating, oxygen ($\delta^{18}O$), carbon ($\delta^{13}C$), and strontium ($^{87}Sr/^{86}Sr$) isotopic values, and elemental concentrations indicate that travertine deposits within the Yellowstone caldera formed during three main episodes that correspond broadly with known periods of wet climate: 13.9–13.6 ka, 12.2–9.5 ka, and 5.2–2.9 ka. Travertine deposition was in response to the influx of large volumes of cold meteoric water that increased the rate of chemical weathering of surficial sediments and recharge into the hydrothermal system. The small volume of intra-caldera travertine does not support a massive postglacial surge of CO_2 within the Yellowstone caldera nor is magmatic CO_2 the catalyst for postglacial travertine deposition.

INTRODUCTION

Volcano-hydrothermal systems evolve over time in direct response to magmatic, tectonic, and climatic forcings that dictate rates of water recharge, thermal fluid circulation patterns, and thermal dissipation. Understanding which factors are the most influential in active, unexhumed hydrothermal systems is often difficult without a temporal perspective on how the system responds to known internal and external forces. Fortunately, the chemistry of thermal waters and their mineral deposits provide a window into the evolution of hydrothermal systems (Hurwitz and Lowenstern, 2014 and references therein). The location, volume, and deposition rate of travertine provide a record of hydrothermal changes over annual to millennial time scales since the late Pleistocene (Fig. 1; Barger, 1978; Sturchio et al., 1994; Fouke et al., 2000; Fouke, 2011; Chafetz and Guidry, 2003; De Boever et al., 2021). The most well-known and studied travertine deposit in Yellowstone National Park is at Mammoth Hot Springs (Bargar, 1978; Pierce et al., 1991), but travertine is also deposited within the Yellowstone caldera in the Upper and Lower Geyser Basins and near the southern boundary of Yellowstone National Park (Fig. 1).

Small travertine deposits (<50 m in length and only several meters high) within the Yellowstone caldera are associated with thermal springs that are not currently depositing travertine or are extinct. The subsurface within the Yellowstone caldera consists of thick rhyolite flows and ignimbrites that are poor in calcium (Christiansen, 2001), so thermal waters discharging at hot springs are mostly at near-saturation with respect to silica (SiO_2), not calcium carbonate. The existence of travertine within the caldera, therefore, is puzzling and requires hydrochemical conditions that are not presently typical for the major intra-caldera geyser basins.

Mechanisms driving past travertine deposition within the Yellowstone caldera could have originated at either shallower or deeper levels within the hydrothermal system (Fig. 2). A potential shallow mechanism could have been large influxes of cold meteoric water into the hydrothermal system that cooled groundwater temperatures and increased calcium concentrations. This meteoric water could have originated as meltwater from Pinedale glaciers, which at their maximum extent from 22–14.5 ka covered the Yellowstone Plateau in up to a kilometer of ice (Bargar and Fournier, 1988; Licciardi and Pierce, 2018), or as rainfall during prolonged wet periods (centennial to millennial scale in duration; Fig. 2a). Alternatively, travertine deposition may have been catalyzed by the release of subsurface carbon dioxide either from postglacial crustal decompression, seismic events releasing accumulated crustal volatiles (Fig. 2b), or degassing of shallow (<5 km depth) magmatic intrusions (Fig. 2c). As there have been no known volcanic eruptions since ~70 ka (Christiansen, 2001; Stelten et al., 2023), localized spikes in CO_2 from magmatic degassing of shallow intrusions (<5 km depth) are ruled out. Therefore, the timing of hydrothermal travertine deposition within the Yellowstone caldera is related to postglacial climate and/or the occurrence of past seismic events. This study uses ^{230}Th-U ages, isotopic values of carbon ($\delta^{13}C$), oxygen ($\delta^{18}O$), strontium ($^{87}Sr/^{86}Sr$), and the

elemental compositions of travertine deposits within the Yellowstone caldera to understand the role of different external forces in triggering deposition of these unique intra-caldera travertine deposits.

GEOLOGY AND STUDY REGION

The term travertine in this study refers to non-marine carbonates ($CaCO_3$ as calcite and aragonite) precipitated from groundwater discharged at thermal springs (Fouke et al., 2000). In the Yellowstone hydrothermal system, circulating groundwater is heated by the magmatic system, rises along crustal faults and permeable zones such as the edges of rhyolite flows, where it may mix with cool meteoric water or boil, and discharges at hot springs (Fournier, 1989; Hurwitz and Lowenstern, 2014). Upon discharge, reductions in both pressure and temperature result in exsolution of dissolved CO_2, supersaturating waters with carbonate species and triggering mineral precipitation (Friedman, 1970). Modern travertine-depositing waters in Mammoth Hot Springs discharge at temperatures of ~70°C, which is below the boiling point of pure water for their elevations (93–94°C). The source of calcium and carbonate to Mammoth Hot Springs originates from the dissolution of Paleozoic and Mesozoic limestones and evaporites in the subsurface (Pierce et al., 1991). The travertine deposits described in this study are within the 631 ka Yellowstone caldera and are located in the Upper Geyser Basin (near Morning Glory Pool and the Hillside Springs Group), the Lower Geyser Basin (east of Firehole Lake), and at Terrace Spring near Madison Junction (Waldrop and Pierce, 1975; Waldrop, 1975; Muffler et al., 1982a, 1982b; Fig. 1). These deposits precipitated subaerially, supported by the ubiquitous presence of finely laminated beds (rather than the poor bedding typically found in tufas) and the large crystal size and euhedral habit (shrubs, spars, dendrites, blades, or shards) of carbonate grains (Capezzuoli et al., 2014). Present-day climate in the Upper and Lower Geyser Basins is

best approximated using the Old Faithful climate station, whose records span from 1904 to the present (https://wrcc.dri.edu/cgi-bin/cliMAIN.pl?wy6845). Average temperatures over the period of record were -9.8°C in January, 14.0°C in July, and 1.3°C annually. Precipitation is high in December-January and May-June. Much of the precipitation falls as snow (November–March), while summers (July–September) are relatively dry. The highest discharge of the Firehole River (whose catchment includes all the Upper and Lower Geyser Basins) occurs in May and June from the melting of winter snowpack.

Firehole Lake Travertine, Lower Geyser Basin

Firehole Lake (2250 masl) is located on the far eastern side of the Lower Geyser Basin in a narrow valley between the Mallard Lake and Elephant Back rhyolite flows (Fig. 1B; supp. Fig. 5). Several hot springs are currently active on the banks of Firehole Lake, which is itself a thermal feature. The travertine deposit is east of these active features and forms a wide low-relief, flat-topped set of terraces that covers an area roughly 185 by 60 meters. The travertine in many spots is brown from co-precipitation of manganese oxides and carbonates with the travertine, and in some locations thin layers of calcite are interspersed with thin layers of manganese oxides and carbonates. The exposed section of the deposit is estimated to be ~3.3 m thick.

Hillside Springs Travertine, Upper Geyser Basin

The Hillside Springs Group is an active set of springs that discharge from the Summit Lake rhyolite flow; they are the westernmost springs in the Upper Geyser Basin (Fig. 1C; supp. Fig. 2). The springs issue from high on a hillside (2280 masl) and have deposited both carbonate and silica minerals, although they do not precipitate appreciable amounts of either mineral at present (Allen and Day, 1935). Large outcrops of older travertine can be found below (2234–

2264 masl) the currently active springs where they form dissected and eroded mound- and fissure-type structures of low relief. The exposed thickness of these deposits is less than four meters. An isolated spring approximately 500 m northwest of the main Hillside Springs Group actively discharges at 2251 masl and is associated with another deposit of travertine (supp. Fig. 3). The mound here is 4 m wide by 2.5 m high and exhibits a transition from layers exclusively of 0.5–2 cm thick travertine to the top meter exhibiting interlayered silica sinter and travertine.

Travertine Near Morning Glory Pool, Upper Geyser Basin

Travertine deposits in a small draw ~400 meters north of Morning Glory Pool (2247 masl) on the east side of the Upper Geyser Basin form a single low, flat-topped terrace that is not associated with any active thermal springs (Fig. 1D, supp. Fig. 4). This travertine deposit is roughly 53 by 22 m in size, centered within a drainage where paleowaters issued through unconsolidated Pinedale-age glacial till (Waldrop, 1975; Muffler et al., 1982b). The travertine is layered with prominent, 15- to 30-cm thick beds of hard, dense travertine that is in turn composed of thinner layers a few millimeters to 1.5 cm thick, all of which are buff to pinkish in hue. The exposed thickness is less than one meter.

Terrace Spring Travertine, Caldera Boundary

Terrace Spring (2100 masl) is a currently active hot spring pool just north of Madison Junction located at the intersection of the youngest caldera rim fault with major north-south trending faults of the Norris-Mammoth corridor (supp. Fig. 1). The pool is usually characterized by vigorous bubbling due to the very high flux of CO_2 (Lowenstern et al., 2005) and temperatures below boiling (~50°C maximum measured in July 2021). Travertine deposits spread out on a wide, low sloping plain east and downhill of the currently active springs, forming

138 flat terraces, low outcrops dispersed in a grassy field, and small low benches of old terrace
139 cascades. Exposed stratigraphy is estimated to be no more than half a meter.

140 **METHODS**

141 We identified and sampled travertine over three field seasons. Thin sections were cut and
142 examined under plane and cross polarized light to identify travertine textures, accessory
143 minerals, and lithics. Small ~50-100 g pieces of fresh travertine were analyzed for major and
144 minor element concentrations using x-ray fluorescence (XRF) on a Perform'X X-ray
145 fluorescence spectrometer at Hamilton Analytical Laboratory at Hamilton College, New York.
146 Fused discs were analyzed for trace element concentrations using a laser-ablation inductively
147 coupled plasma mass spectrometer (LA-ICP-MS) at the Colorado School of Mines (detailed
148 methods and data in Harrison et al., 2023).

149 Rock slabs were cut perpendicular to bedding surfaces and polished to expose fine
150 structures. Small aliquots (40-150 mg) of material from single travertine layers were excavated
151 with a dental drill under a binocular microscope, avoiding areas of diagenetic alteration (e.g.,
152 euhedral crystals in voids; recrystallized areas along bedding planes; areas with different
153 fluorescent properties when viewed under shortwave infrared light; see supplementary
154 information and Harrison et al., 2023) and contamination with detrital material. Aliquots of this
155 powder were analyzed for stable oxygen and carbon isotopes, as well as for strontium, uranium,
156 and thorium isotopes. Oxygen and carbon isotope values were measured at the U.S. Geological
157 Survey Reston Stable Isotope Lab in Reston, Virginia, using standard techniques (method details
158 in Harrison et al., 2023). Oxygen isotope ratios are reported as $\delta^{18}O$ relative to the Vienna
159 Standard Mean Ocean Water (VSMOW) calculated as $([^{18}O/^{16}O_{sample}]/[^{18}O/^{16}O_{standard}]-1)x1000$

(Coplen, 1994). Carbon isotope results are reported as $\delta^{13}C$ relative to Vienna Peedee Belemnite (VPDB) calculated as $([^{13}C/^{12}C_{sample}]/[^{13}C/^{12}C_{standard}]-1)x1000$ (Coplen, 1994).

Th and U isotope dilution measurements were determined on 20-40 milligram aliquots of travertine powders at the USGS Denver Radiogenic Isotope Lab. Samples were spiked with a high-purity ^{233}U- ^{236}U-^{229}Th tracer solution prior to hot plate digestion using ultra-pure acids. U and Th were separated and purified on ion exchange columns using Bio-Rad AG1×8 anion resin and analyzed on a Thermo-Finnigan Triton multicollector thermal ionization mass spectrometer (TIMS) using peak-jumping on a single electron multiplier (method details, standard values, and measured reference material results are given in Paces et al., 2022 and Harrison et al., 2023).

Initial $[^{234}U/^{238}U]$ values were close to 1 for all samples (mostly 1.02-1.16), similar to values measured in modern thermal waters (1.05–1.07 for Hillside Group Springs, 1.031 for Morning Glory Pool, 1.033 for Terrace Spring; Paces et al., 2022). In addition, uranium isotopic values do not correlate with ages and none of the samples had ^{230}Th-U ages older than the last glacial period (~22-14.5 ka); both findings indicate that significant post-depositional open-system behavior did not occur.

Strontium was separated from the same analytical aliquots as U-series isotopes and purified using Sr-spec resin. Unspiked strontium isotopes were also measured on the same multicollector TIMS using triple-jump, multidynamic analyses (Paces et al., 2022; Harrison et al., 2023).

RESULTS

We report new chemical and isotopic analyses for 64 travertine layers from 36 samples. Data and detailed description of the methods are available in Paces et al. (2022) and Harrison et al. (2023). Most samples, except those near Morning Glory Pool, have $[^{230}Th/^{232}Th]$ values

(square brackets denote activity ratios) greater than 10, which result in robust ^{230}Th-U disequilibrium ages requiring only minimal corrections for common Th (i.e., ^{232}Th plus associated ^{230}Th contributed from a non-authigenic detrital component). Samples from near Morning Glory Pool have high concentrations of ^{232}Th and elements found in detrital silicates (Al, Zr, and chemical index of alteration or CIA elements) that indicate the deposits incorporated a larger component of silicate dust or dissolved salts during their formation relative to other travertines in this study. Because some of the ^{230}Th present in travertines with elevated ^{232}Th is exogenous and not supported by radiogenic decay of uranium present in the samples, ^{230}Th contributions from the detrital component must be mathematically subtracted from the analysis; this results in larger uncertainties in ^{230}Th-U ages (Ludwig and Paces, 2002).

^{230}Th-U age results show three main episodes of travertine deposition within the Yellowstone caldera (Fig. 3). The first interval occurred soon after recession of Pinedale glaciers between 13.9–13.6 ka and is only recorded in the stratigraphically deepest deposits at Hillside Springs. Following this, a major period of deposition occurred from 12.2 to 9.5 ka at Hillside Springs and near Morning Glory Pool followed by a ~4 ka hiatus during much of the early Holocene. Travertine precipitation ceased completely at the main Hillside Springs and near Morning Glory Pool after the second depositional episode, but late-Holocene precipitation occurred at North Hillside between 5.2 and 3.9 ka, followed closely by travertine deposition near Firehole Lake from 3.8 to 3.0 ka. The veneer of travertine deposited near Terrace Spring is ~1.2 ka.

The Hillside Springs travertines are divided into three groups (Old Hillside, Hillside, and north Hillside) that are spatially and temporally distinct (Fig. 1C). The older Hillside Springs travertines have ages >13.5 ka and are stratigraphically the deepest. The main Hillside Springs

deposit forms a continuous stratigraphic section best exposed at the southernmost end of the thermal area and has ages between 12.2 and 11.1 ka. An isolated thermal feature and travertine deposit at North Hillside (0.5 km north of the other Hillside Springs thermal features) formed between 5.2 and 3.9 ka and has no exposed travertines that correlate with the older Hillside Springs deposits.

Travertine deposits from different locations and ages tend to cluster into groups with similar strontium and oxygen isotopic values (Fig. 4, Fig. 6). Travertine $^{87}Sr/^{86}Sr$ vary between 0.70979 and 0.71079 and do not show obvious temporal trends. Instead, samples from different locations tend to have similar $^{87}Sr/^{86}Sr$ values that cluster over narrow and distinct ranges (Fig. 6). The $\delta^{18}O$ values vary between -1.25 and 9.37‰, with older travertines broadly exhibiting lower $\delta^{18}O$ values and younger travertines exhibiting higher values (Fig. 4). Similarly, older travertines have higher relative magnesium content and chemical indices of alteration (CIA) than younger travertines (Fig. 5). CIA is defined as $CIA = [Al_2O_3/(Al_2O_3 + CaO^* + Na_2O + K_2O)] \times 100$ where all oxides are calculated as molar oxides and CaO* is calcium oxide in the silicate fraction only, here calculated using $CaO = Na_2O$. In this study, CIA is used as an indication of removal of mobile cations during chemical weathering, facilitated by high chemical weathering that accompanies the transition from glacial to interglacial epochs (Wang et al., 2020). The $\delta^{13}C$ values vary between -0.70 and 4.23‰; travertines from different locations tend to cluster around similar values (Fig. 4).

DISCUSSION

Controls on Travertine Deposition in the Yellowstone Hydrothermal System

Sources of bicarbonate and calcium are necessary for travertine deposition. There are several sources of CO_2, and therefore bicarbonate, to the Yellowstone hydrothermal system. One

source is basaltic magma deep within the crust and subsequent crystallization of more evolved magma bodies at shallower crustal levels (e.g., long-lived magma reservoirs between ~5–17 km depth; Fournier, 1989; Werner and Brantley, 2003; Moran et al., 2017). Another possible source is from decomposition of carbonate-rich sedimentary rock underlying Quaternary volcanic units, although limestones originally beneath the present-day caldera have likely been at least partially consumed during the 2.2-million-year lifetime of Yellowstone volcanism (Christiansen, 2001; Lowenstern et al., 2015). Another possible source of CO_2 is decomposition of organic material; however, within the Upper and Lower Geyser Basins, input of CO_2 from biotic sources is assumed to be negligible based on ratios of CH_4 to higher-order organic compounds (i.e., ethane, propane, butane, etc.) that are less than 1000 in fumarole gases (Bergfeld et al., 2014; Moran et al., 2017). Regardless of where CO_2 originates, the hydrothermal system buffers inputs of deep CO_2 by dissolution into thermal fluids and precipitation of secondary minerals in the deep subsurface during steam separation via the generalized reaction:

$$HCO_3^-{}_{(aq)} + Ca^{2+}{}_{(aq)} \leftrightarrow CaCO_{3(s)} + CO_{2(g)} + H_2O_{(l)} \qquad \text{(eq. 1)}$$

The deposition of travertine at the surface occurs when CO_2 exsolves from groundwater due to a reduction in the partial pressure of CO_2 (pCO_2) as spring discharge approaches atmospheric pressure. Temperature, pH, and the concentrations of Ca^{2+}, Mg^{2+}, HCO_3^-, and $SO4^{2-}$ are likely important parameters controlling the precipitation of the calcium carbonate ($CaCO_3$) minerals in travertine deposits (Luo et al., 2022). The concentrations of Ca and Mg in the alkaline waters of the geyser basins today are typically less than 1 mg/l and 0.05 mg/l, respectively (McCleskey et al., 2022) and are too low for carbonate saturation. The travertine deposits investigated in this

252 study are located at the margins of the Upper and Lower Geyser Basins where spring
253 temperatures are typically below boiling, the concentrations of Ca^{2+} and Mg^{2+} are slightly higher,
254 the Cl^- and SiO_2 concentrations are lower, and the HCO_3^- concentrations are comparable to or
255 higher than the central parts of the basins where most springs discharge at boiling temperature.
256 The postglacial episodes of intra-caldera travertine deposition most likely resulted from
257 either higher CO_2 concentrations (as bicarbonate, HCO_3^-), higher Ca^{2+} and Mg^{2+} concentrations,
258 or both in paleo groundwater compared with concentrations in modern groundwater. Increases in
259 CO_2 into the deep hydrothermal system would have driven dissolution of calcite at depth and
260 resulted in higher concentrations of Ca^{2+} and HCO_3^- in thermal waters according to equation 1.
261 This increased flux could have originated from concurrent shallow degassing of basaltic
262 intrusions, as has been hypothesized on the Colorado Plateau (Priewisch et al., 2014). However,
263 there is no evidence for late-Pleistocene shallow (<5 km depth) basaltic magma intrusions in the
264 Yellowstone Plateau Volcanic Field (Christiansen, 2001), nor is there evidence for large deposits
265 of travertine that would have been produced by such intrusion(s) (see section 4.4). Instead,
266 pulses of travertine deposition likely track greater influxes of Ca^{2+} and Mg^{2+} into the
267 hydrothermal system.
268 Pinedale ice recession was well underway in the northern, eastern, and southern parts of
269 the region from 18–14.5 ka based on the ages of moraines around Yellowstone Plateau (Licciardi
270 and Pierce, 2018, Fig. 7B). The melting of the ~1 km thick Yellowstone ice cap would have
271 produced large volumes of water charged with high total dissolved solids due to supercharged
272 rates of silicate weathering driven by production of highly particle-reactive glacial flours and
273 sediments (Wang et al., 2020). This geochemical signature is observed as elevated Mg
274 concentrations in the oldest, ~14 ka Hillside travertine deposits (Fig. 5A). The influx of

meltwater into the shallow hydrothermal system in addition to providing additional Ca^{2+} would have lowered water temperatures. Lower temperatures of groundwater in the shallow hydrothermal system would have suppressed subsurface thermal fluid boiling and associated loss of gaseous CO_2. Consequently, the equilibrium in Equation 1 is driven toward the left resulting in decreased calcite precipitation and sequestration of calcium in the subsurface. Cooler temperatures also would have increased the reactivity of thermal waters with subsurface rhyolite flows, which is more effective at temperatures below 275°C, further boosting calcium concentrations in discharging thermal waters (Bischoff and Rosenbauer, 1996; Cullen et al., 2019).

This regime lasted as long as the large volumes of cold, meteoric water increased surficial weathering and supplied recharge with higher total dissolved solids (Fig. 2A). As the glaciers disappeared and surficial conditions dried, cold meteoric water infiltration decreased and thermal waters became less reactive with subsurface rhyolite due to the higher temperatures of water-rock interaction. Higher thermal water temperatures also resulted in more boiling and calcite precipitation in the deeper subsurface, further decreasing concentrations of calcium and bicarbonate ions in thermal waters discharging at the surface. Consequently, Ca^{2+} and total alkalinity concentrations would have declined to a point where calcite saturation could not be maintained, similar to modern hydrothermal conditions within the Yellowstone caldera where travertine deposition does not occur.

Although the scenario of intra-caldera travertine deposition illustrated above uses the high meltwater volumes produced during glacial recession as the source of cold water to the hydrothermal system, the same processes would operate if extended periods of high precipitation caused substantial increases of meteoric recharge to the Yellowstone hydrothermal system. This

298 concept is supported by data from frequent sampling of rivers that drain thermal areas in the
299 Yellowstone caldera. The ratios of HCO_3^-/Cl^- and Ca^{2+}/Cl^- and the total discharge of HCO_3^- and
300 Ca^{2+} increase substantially during elevated fluvial discharge following annual snowmelt
301 (Hurwitz et al., 2010). This observation suggests that more meteoric recharge into the subsurface
302 increases the concentrations of HCO_3^- and Ca^{2+} in groundwater, which, when scaled to higher
303 precipitation levels than observed during historical monitoring, may significantly increase the
304 propensity for travertine deposition.
305 Finally, evidence for the calcite buffering capacity of the subsurface hydrothermal system
306 is illustrated by the oxygen isotope composition of hydrothermal minerals analyzed from several
307 research cores drilled in the Upper and Lower Geyser Basins in the late 1960s (White et al.,
308 1975). The stable isotope composition of hydrothermal quartz and clay minerals at depth was not
309 in equilibrium with the $\delta^{18}O$ of present-day thermal waters, whereas that of calcite was in
310 equilibrium (Sturchio et al., 1990). This discrepancy suggests that quartz and clays are unreactive
311 over time and chemical changes in the hydrothermal system, whereas calcite is continuously
312 dissolved and precipitated with changing hydrothermal conditions, cycling with the amount of
313 CO_2 and Ca^{2+} supplied and temperature of the reservoir.
314 **Travertine Stable Isotope & Geochemical Signals**
315 ***Travertine Elemental Compositions: Higher Rates of Surficial Weathering in the Past***
316 Pinedale Glaciation spanned from ~22 to 14.5 ka on the Yellowstone Plateau based on
317 cosmogenic nuclide exposure dating of ice-marginal features and radiocarbon dating of
318 postglacial lake sediments (Licciardi and Pierce, 2018; Whitlock, 1993). Subaerial travertine
319 deposition was initiated at Hillside Springs at about 13.9 ± 0.12 ka, providing a minimum age for
320 glacial recession in the Upper Geyser Basin. The elevated chemical alteration index (CIA) with

low Ca/(Ca+Mg) and $\delta^{18}O$ of Old Hillside Springs travertines suggests deposition from waters that contained a significant component of surficial glacial meltwater (Fig. 5).

The low Ca/(Mg+Ca) ratio in postglacial travertines is a result of the weathering of exotic glacially transported sediment (Fig. 5A). Because high-silica rhyolites underlying the Yellowstone caldera are Ca- and Mg-poor, sediments with higher calcium and magnesium are required to explain the elevated magnesium concentrations in the oldest Hillside travertines. A good source for these sediments would have been the basaltic and andesitic Absaroka volcanics located in the northeastern sector of the Yellowstone region, transported west by glaciers that originated northeast or east of Yellowstone National Park in the Beartooth uplift or volcanic Absaroka Range (Licciardi and Pierce, 2018). Substantial deposits of Pinedale-age till and glacial kame in Upper and Lower Geyser Basins confirms the occurrence of locally high sedimentation rates in postglacial time, as does carbonate-bearing Pinedale-age loess deposits in Jackson Hole, Wyoming (Waldrop, 1975; Waldrop and Pierce, 1975; Muffler et al., 1982a; 1982b; Pierce et al., 2011). Significantly, Pinedale-age loess exhibits significant calcium and magnesium leaching in the top two meters, indicating that snowmelt and precipitation in postglacial times was high enough to extensively leach labile elements from fresh reactive deposits (Pierce et al., 2011). Similarly high rates of sedimentation from glacial outwash are also recorded in Blacktail and Slough Creek ponds in northern Yellowstone National Park (Krause and Whitlock, 2013; Whitlock et al., 2012).

Travertine Stable Isotopes: Variations in Paleowater Composition

The $\delta^{18}O$ values of paleowaters that deposited travertine were likely 2–4‰ lower than present-day surficial waters within the Upper Geyser Basin (approximately -18.2‰ at Hillside Springs; McCleskey et al., 2022), indicating either a glacial meltwater source (-23 to -25‰ for

Pleistocene ice; Bindeman and Lowenstern, 2016) or cold late-glacial precipitation (2-4‰ lower than present-day precipitation based on isotope measurements of fossilized teeth in the western U.S.; Kohn and McKay, 2010).

To assess the stable isotope compositions of travertines, we calculate the theoretical $\delta^{18}O$ that would be in equilibrium with present-day thermal waters at Hillside Springs ($\delta^{18}O_{water} \approx$ -18.2‰; McCleskey et al., 2022) using the fractionation factor-temperature equation of Kele et al. (2015), which was calibrated for temperatures up to 90°C. The maximum temperature a travertine can precipitate subaerially is 92°C, which is the boiling temperature of pure water at the local elevation. Travertine formed from water with $\delta^{18}O_{water}$ = -18.2‰ at this temperature has an equilibrium $\delta^{18}O_{carbonate}$ of 0.40‰. This value is too high to account for the lowest $\delta^{18}O_{carbonate}$ of the late-Pleistocene travertines from Hillside Springs and some of the oldest travertines from near Morning Glory Pool (Fig. 4C). Furthermore, travertines typically precipitate from waters that are 10–30°C cooler than the boiling temperature, further increasing the value of equilibrium travertine $\delta^{18}O_{carbonate}$. Other processes in this system, including reactions between meteoric waters and subsurface rhyolite ($\delta^{18}O_{rhyolite} \approx$ 6‰; Bindeman and Lowenstern, 2016) and steam separation at depth will further increase the thermal water $\delta^{18}O_{water}$ to more positive values (McKenzie and Truesdell, 1977). Therefore, it is impossible to explain the $\delta^{18}O_{carbonate}$ of the oldest travertines without requiring much lower $\delta^{18}O_{water}$ in the recharge water, to allow values down to -22‰ in discharging paleowaters. To illustrate, the calculated $\delta^{18}O_{water}$ of paleowaters in equilibrium with measured $\delta^{18}O_{carbonate}$ values at a reasonable temperature range of 70−80°C requires $\delta^{18}O_{water}$ values between -19.5 and -22.2‰ for Old Hillside (Fig. 4C). If these calculated $\delta^{18}O_{water}$ are plotted on the global meteoric water line with modern Yellowstone cold surface waters, the paleowaters that formed Old Hillside, some of the Hillside Springs, and near Morning

Glory Pool travertines were lower in deuterium and oxygen isotopic values than any known modern precipitation source (Rye and Truesdell, 2007; Fig. 4D). For comparison, all modern Mammoth Hot Spring travertines have a $\delta^{18}O_{carbonate}$ = 1.88−9.61‰, which were deposited from 28−73°C waters that have $\delta^{18}O_{water}$ values between -16.6 and -18.3‰. These modern calcite values are comparable to those measured in younger travertines from North Hillside, Firehole Lake, and Terrace Spring (Friedman, 1970; Chafetz and Lawrence, 1994; Fouke et al., 2000; Fig. 4A).

The $\delta^{13}C_{carbonate}$ values vary between -0.70‰ at North Hillside and 4.23‰ in near Morning Glory Pool travertines, with no consistent trend with time (Fig. 4). The Yellowstone ecosystem is dominated by C3-type vegetation and has been since deglaciation, resulting in no drastic variations in $\delta^{13}C$ from the transition from late-glacial tundra to present-day forest. Consistent travertine $\delta^{13}C$ values through time and between the different intra-caldera travertine deposits indicate that the source of carbon to thermal waters was dominated by deep sources of carbon, not shallow ones that likely would have varied isotopically with differences in climate, soil respiration, and vegetation. Most (78%) modern diffuse soil CO_2 $\delta^{13}C$ isotope values are in the range of Yellowstone fumarole gases, which are slightly lower than the $\delta^{13}C$ values of most intra-caldera travertine (Moran et al., 2017; Werner and Brantley, 2003; Rahilly and Fischer, 2021). These data are evidence that a major source of CO_2 in thermal waters is magmatic gas from the deep long-lived Yellowstone magmatic reservoir that produces a dispersed and relatively constant flux across the Yellowstone Plateau Volcanic Field (Fig. 4; Moran et al., 2017; Werner and Brantley, 2003; Rahilly and Fischer, 2021). It is impossible to resolve with stable carbon and oxygen isotopes whether the $\delta^{13}C_{carbonate}$ of intra-caldera travertines is a result of mixing between this deep magmatic gas ($\delta^{13}C$ = -3; $\delta^{18}O$ = -21) and sedimentary rocks in the

subsurface (average $\delta^{13}C = 0.6$; $\delta^{18}O = 20$) followed by kinetic fractionation of carbon isotopes driven by rapid subaerial CO_2 degassing or boiling of subsurface fluids followed by kinetic fractionation with subaerial CO_2 degassing (Fig. 4B). We find it likely that the first scenario is more probable given that any significant subsurface boiling would have precipitated calcium carbonate underground and therefore may not have resulted in surficial travertine deposits. It should be noted that Mammoth Hot Spring travertines have higher $\delta^{18}O_{carbonate}$ and $\delta^{13}C_{carbonate}$ values that trend towards the composition of Madison Limestone rocks of Mississippian age (Fig. 4B; Pierce et al., 1991; Kharaka et al., 1991) and therefore Mississippian-age seawater values, an indication of greater sedimentary input north of the caldera than within it (Fig. 4B). The transition from the vent to pond to distal facies of Mammoth Hot Springs travertine shows 2.3‰ variation in $\delta^{13}C$ and 4.6‰ variation in $\delta^{18}O$ over 6 meters because of degassing of isotopically light CO_2 along the flow path (Fouke et al., 2000), an observation consistent with rapid kinetic isotopic fractionation with surficial CO_2 degassing (vertical trend in Fig. 4B).

Travertine Strontium Isotopes: An Indication of Subsurface Water Flow Path

Thermal water plumbing paths of paleowaters for each travertine deposit are inferred from the $^{87}Sr/^{86}Sr$ isotopic composition of travertines (Fig. 6). Water rock reaction and carbonate precipitation is understood to not cause strontium isotopic fractionation, so the isotopic composition of discharging thermal waters and travertines is a record of the strontium isotopic composition of the rock, or at least the most leachable fraction of the rock, with which the water equilibrated. The uniform Sr isotopic composition for each group of travertines from different locations supports this assumption and indicates that the plumbing paths for each travertine thermal system was unique.

The pathway of groundwater discharge that produced the travertine near Morning Glory Pool was very different from present-day thermal waters in the Upper Geyser Basin, based on the much higher $^{87}Sr/^{86}Sr$ of present-day thermal waters than the near Morning Glory Pool travertines. Instead of being fed by the main thermal fluid upflow in the Upper Geyser Basin, which likely equilibrated with the underlying Biscuit Basin rhyolite flows (Fig. 6A), thermal waters responsible for the near Morning Glory Pool travertine likely equilibrated with the Lava Creek Tuff (Fig. 6B), known to be cryptically and heterogeneously present in the shallow subsurface in uplifted fault blocks (Keith and Muffler, 1978), rather than the nearby Mallard Lake flow with lower $^{87}Sr/^{86}Sr$. Terrace Spring $^{87}Sr/^{86}Sr$ isotope values are also consistent with a flow path through the Lava Creek Tuff, which is unsurprising given that this spring discharges from the base of a cliff of Lava Creek Tuff on the caldera ring fault (Waldrop and Pierce, 1975). The other travertines are similar in strontium isotopic composition to rhyolite flows of the Central Plateau Member of the Plateau Formation or the Mallard Lake flow of the Upper Basin Member of the Plateau Formation, indicating flow paths through these units, likely in the highly permeable autobrecciated contact zones between flows (Finn et al., 2022). Equilibration of thermal fluids with the more reactive glass may have resulted in thermal water $^{87}Sr/^{86}Sr$ isotopic values that were slightly lower than the whole rock because the glasses of some rhyolite flows are slightly more primitive than their crystal cargo from the injection of more mafic magma shortly prior to eruption (Loewen et al., 2017).

Travertine Deposition Timing: Climatic and Tectonic Connections

The late Pleistocene (14.5–10 ka): Deglaciation & the Younger Dryas

The initial postglacial deposition of travertine at Hillside Springs occurred from 13.9 to 13.5 ka and closely post-dates cosmogenic exposure ages of late-Pinedale recessional moraines

435 located both north and south of the geyser basins (Licciardi and Pierce, 2018; Fig. 7B). Because
436 ice recession was likely from west to east over the Upper and Lower Geyser Basins, the lack of
437 travertine dating to 13.9–13.5 ka on the eastern side of the basins may indicate that they were
438 still covered by ice, there was active glacial outwash at this time that prevented or buried
439 travertine deposits, or that deposits of this age are no longer exposed. At Hillside Springs,
440 travertine deposition ceased after approximately 500 years, suggesting that the effects of glacial
441 meltwater infiltration were short-lived or surficial conditions prevented travertine deposition
442 and/or preservation between 13.5–12.2 ka.

443 Based on the current sampling resolution, more voluminous deposition of travertine
444 commenced at 12.2 ± 0.2 ka at Hillside Springs, an episode that appears to have commenced 700
445 years into the Younger Dryas cold event (~12.9–11.7 ka; Cheng et al., 2013) and continued until
446 9.5 ka (Fig. 3). Travertines ages do not align with the beginning of the Younger Dryas, which
447 suggests that: 1) the Yellowstone hydrothermal system response lagged behind a climate trigger
448 by hundreds of years; 2) cooling was not strongly registered in this region before 12.2 ka; or 3)
449 the early part of the Younger Dryas was cool but not sufficiently wet. It is also possible that the
450 Yellowstone hydrothermal system has a significant buffering capacity (via the precipitation and
451 dissolution of subsurface calcite) and requires sustained, high inputs of meteoric water to impact
452 thermal water chemistry. All travertine deposits investigated here are located near the edges of
453 geyser basins. Their location suggest that chemical transformations of discharging groundwater
454 were confined to the edges of geyser basins, where mixing between cool meteoric-water-fed
455 aquifers and upwelling basin thermal waters was greatest (e.g., Finn et al., 2022) and where the
456 maximum temperatures of recharge waters heated in the subsurface would be lowest.

The climate and environment of the Yellowstone region during the Younger Dryas cold period is poorly known. Some, but not all, cirque glaciers in the Wind River Mountains (Gosse et al., 1995; Dahms et al., 2018), Beartooth Mountains (Barth et al., 2022), and across the western U.S. (Marcott et al., 2019) experienced readvances or standstills during this time. A standstill moraine at Emerald Lake in the Beartooth uplift, for example, has a low-aspect ratio suggesting a short-lived, minor climate excursion or period of low sediment deposition during a pause in glacial retreat (Barth et al., 2022). Similarly, the youngest exposure age for moraines in the Tetons is attributed to a minor glacial standstill during early Younger Dryas time (Lake Solitude, Fig. 7B; Licciardi and Pierce, 2018). In most cases, regional glaciers did not experience significant advances during Younger Dryas time.

Younger Dryas cooling is also not clearly recorded in pollen records from the Yellowstone region, possibly because: 1) the pollen sampling interval lacks the resolution to capture a short-lived event; 2) the region did not experience significant climate change; or 3) the subalpine mixed-conifer forest at the time was relatively insensitive to cool conditions (Whitlock et al., 2008; 2012; Krause and Whitlock, 2013). Blacktail Pond, located in northern Yellowstone National Park, shows low $\delta^{18}O$ values in authigenic carbonates that indicate less lake-water evaporation along with pollen indicative of treeless vegetation during the Younger Dryas (Krause and Whitlock, 2013).

The initial deglacial landscape of the central Yellowstone Plateau was choked with till, outwash, and loess. As the climate warmed after 13 ka, different conifers started to move into the Yellowstone region and become established. One of the early species, Engelmann spruce (*Picea engelmannii*), colonized between 13 and 11.5 ka at all elevations and apparently at the same time as formation of travertine at Hillside Springs and near Morning Glory (Krause and Whitlock,

2017; Fig. 7C). Soil development and related weathering of sediments were likely important factors for both early forest establishment and travertine formation, reflecting a lag of centuries between deglaciation and sufficient weathering to establish soils and increase the total dissolved solids in infiltrating meteoric waters.

Early- to mid-Holocene (11–5 ka)

Travertine deposition continued until 11.1 ka at Hillside Springs and from approximately 11.7 to 9.5 ka near Morning Glory Pool before hydrothermal systems transitioned back to silica sinter deposition because of the warmer, drier summer conditions of the early to middle Holocene (Whitlock 1993; Larson et al., 2020; Chellman et al., 2021; Schiller et al., 2021). These climatic changes are attributed to the amplification of the seasonal cycle of insolation (Bartlein et al., 1998; Fig. 7A). Travertine deposition seems to have ceased concurrently with climatic drying at Hillside Springs (at 11.1 ka), whereas near Morning Glory Pool travertine deposition did not stop until ~9.5 ka, possibly because its thermal waters were supported by a larger source of calcium and magnesium from recharge through thicker deposits of Pinedale till on the east side of Upper Geyser Basin than the west. It is also noteworthy that Minnetonka Cave, located in the Wasatch Mountains in southeastern Idaho, also ceased depositing speleothem calcite at ~9.5 ka (Lundeen et al., 2013), coincident with cessation of travertine deposition near Morning Glory Pool.

Strong support for warm dry conditions near the geyser basins come from $\delta^{18}O$ data determined from fossil diatoms preserved in Yellowstone Lake cores, which indicate high lake-water evaporation from 9.9 (the beginning of the record) to 7.5 ka (Brown et al. 2021; Fig. 7E). Pollen records from the central and southern Yellowstone region show an expansion of lodgepole pine (*Pinus contorta*) and notable increases in Douglas fir (*Pseudotsuga menziesii*)

503 and aspen (*Populus tremuloides*) between 10 and 5 ka, and a charcoal record from the central
504 Yellowstone region indicates higher fire activity in the early and middle Holocene than at present
505 (Whitlock 1993). Lake levels were also lower than present from 11.3–5.7 ka and especially from
506 9.3–5.7 ka in the Yellowstone and throughout the Rocky Mountain regions (Shuman and
507 Serravezza, 2017; Whitlock et al., 2012; Krause and Whitlock, 2013; Fig. 7D).

508 ***Late Holocene (5 ka–present)***

509 After ~6 ka, decreased summer insolation resulted in cooler, wetter conditions than
510 before, leading to an ecological transformation from open forest to closed forest and from small
511 frequent to large infrequent fires in the central Yellowstone region (Whitlock 1993; Schiller et
512 al., 2021; Fig. 7F). Several paleoclimate proxies indicate cooler and wetter conditions than
513 before. $\delta^{18}O$ data from Yellowstone Lake fossil diatoms register several cool events from
514 5.5–4.5 ka (Brown et al. 2021; Fig. 7E). Other indications of wet conditions starting around 5 ka
515 include cessation of the Minnetonka Cave speleothem, increased rates of travertine deposition in
516 the Salt Lake graben, increases in $\delta^{18}O$ recorded from the Beartooth ice patch that indicate
517 warmer winter temperature and greater snowpack than before, and the rise of Rocky Mountain
518 lake levels, which is consistent with more snowpack and/or less evaporation (Lundeen et al.,
519 2013; Kampman et al., 2012; Shuman and Marsicek, 2016; Chellman et al., 2021; Fig. 7).
520 Deposition of travertine at North Hillside started at 5.2 ± 0.04 ka and lasted approximately 1340
521 years, coinciding with this wetter regional climate.

522 Firehole Lake travertine deposition occurred between 3.8 and 3.0 ka and its onset may
523 have been caused by hydrothermal system reorganization or a continuation of late Holocene wet
524 conditions. It is also important to note that the exposed Firehole Lake travertine may only be the
525 top of a thicker deposit, as is suggested by the presence of travertine between 8–10 m depth in

526 the Y-2 research drill core located less than 50 m west of the sampled surficial deposit (Bargar
527 and Beeson, 1981; Fig. 1B). Regardless of the presence of older travertines, ~3.8 ka coincides
528 with the Minnetonka Cave speleothem ceasing deposition due to cool, wet conditions, the
529 Beartooth ice patch greatly increased ice accretion due to cooler conditions with continued high
530 precipitation, lakes showed a modest decrease in lake levels, and the Salt Lake graben
531 experienced the highest deposition rates of its record (Lundeen et al., 2013; Kampman et al.,
532 2012; Shuman and Marsicek, 2016; Chellman et al., 2020; Fig. 7).
533 Geochemical, pollen, and diatom records from nearby Goose Lake in Lower Geyser
534 Basin (Schiller et al., 2021) show a sharp decline in arsenic concentrations and cooler water
535 conditions at 3.8 ka, which is interpreted as evidence of thermal water ceasing to flow into Goose
536 Lake. This shift in hydrothermal activity coincided with the opening of the forest and less fire
537 activity in the Lower Geyser Basin and the deposition of Firehole Lake travertine (Schiller et al.,
538 2021; Fig. 7G). The coincidence of travertine deposition at Firehole Lake with hydrothermal
539 changes at Goose Lake suggests a possible seismic event that reorganized the hydrothermal
540 plumbing system of the Lower Geyser Basin that could have released a pulse of accumulated
541 CO_2 (Uysal et al., 2009). Alternatively, the unexposed Firehole Lake travertines may have
542 started forming earlier in time, perhaps dating to the earlier North Hillside event at 5.2 ka and
543 cool conditions.
544 After ~3.0 ka, lower $\delta^{18}O_{diatom}$ values from Yellowstone Lake indicate less evaporative
545 effect implying cooler summers and coinciding with the end of Firehole Lake travertine
546 deposition at 3.0 ± 0.07 ka (Brown et al., 2021; Fig. 7E). A period of Neoglacial advances started
547 in the Teton Mountains at 4 ka and ended at about 2.5 ka, after which increases in sedimentation
548 rate indicate lower precipitation conditions (Larson et al., 2020). Concurrently, a decrease in net

549 ice accretion rate in the Beartooth ice patch after 2 ka indicates warming as does the increase in
550 ice patch $\delta^{18}O_{ice}$ values; increases in $\delta^{18}O_{carbonate}$ at Crevice Lake are likely related to less
551 snowpack; and decreases in Salt Lake graben travertine deposition rates imply warming
552 conditions (Chellman et al., 2021; Whitlock et al., 2012; Kampman et al., 2012; Fig. 7).
553 Values of $\delta^{18}O$ in the Yellowstone Lake diatom record were slightly higher from ca. 2 ka
554 to 1 ka indicating periods of more lake-water evaporation during the Roman Warm Period
555 (2.2–1.55 ka) and Medieval Climate Anomaly (1.2–0.7 ka; Brown et al., 2021). This period also
556 includes deposition of the Terrace Spring travertine, which is a thinly exposed veneer
557 constrained to 1.26–1.06 ± 0.01 ka. This period was associated with drought and widespread
558 aridity in western North America, unlikely conditions for travertine formation. However, the
559 deposit is roughly coincident with a large earthquake on the ~25-km-long Eagle Bay fault zone
560 in Yellowstone Lake, where displacements of one meter are evident in lake bottom sediments.
561 The age of this large earthquake is inferred to be ~1.5 ka (Morgan et al., 2022), and substantial
562 shaking on the Yellowstone Plateau could have fractured a pathway for trapped CO_2 gas to
563 escape to the surface, especially in preexisting fault zones. Springs with mantle-derived helium
564 isotopic compositions are typically associated with deep faults that serve as conduits for high
565 CO_2 fluxes and may assist with saturating thermal waters with calcite at the surface (e.g., Uysal
566 et al., 2009). Terrace Spring has among the highest helium isotope compositions observed in
567 Yellowstone National Park ($R_c/R_a \approx 7.9$; Lowenstern et al., 2005) along with exceptionally high
568 CO_2 concentrations. Furthermore, Terrace Spring is located at the intersection of the caldera rim
569 and major north-south trending faults (Bergfeld et al., 2014). These major structural features
570 likely act as high permeability pathways for fluids and volatiles when major seismic events
571 rupture hydrothermally sealed systems (Uysal et al., 2009).

572 The Terrace Spring deposit is interpreted to have precipitated as a result of a short-lived,
573 seismically induced release of CO_2 that led to travertine deposition without substantial changes
574 to thermal water chemistry, as indicated by the fact that the $^{87}Sr/^{86}Sr$ isotopic composition of the
575 travertine is in equilibrium with modern-day Terrace Spring waters (supplementary information).
576 The absence of other intra-caldera travertine deposits at this time suggests that thermal waters in
577 most areas of the Upper and Lower Geyser Basins did not have enough available calcium for
578 travertine formation, regardless of any seismically induced pulses of CO_2 release. Although
579 intra-caldera travertine deposition may have been supported by CO_2 leakage from seismic
580 activity in the past (e.g., Terrace Spring), the main driving force behind travertine deposition was
581 likely the influx of large volumes of cold meteoric water that decreased the temperature of water-
582 rock reactions and increased the rate of chemical weathering of surficial sediments as is shown
583 by the correspondence between timing of travertine deposition with wet climatic conditions.

584 **Travertine Deposit Volume & CO_2 Flux**

585 The pulsed timing of intra-caldera hydrothermal travertine that corresponds with wet
586 climate indicates that the flux of CO_2 within the Yellowstone caldera was relatively constant in
587 postglacial time and that there was not a large, ephemeral release of CO_2 associated with
588 deglaciation. Furthermore, the small volume of the travertine deposits within the caldera implies
589 a limited spatial and temporal CO_2 flux (Table 1). To examine if an episodic large release of CO_2
590 could have triggered travertine deposition, we first calculate the total volume of intra-caldera
591 travertine deposits. Assuming a travertine bulk density of 2.43 g/cm^3 and a rough travertine
592 volume based on mapped exposures and estimated thickness, the total amount of travertine in the
593 Upper and Lower Geyser Basins is 0.0007 km^3. This amount, when converted from calcite into
594 CO_2 according to equation 1 and following the method of Mancini et al. (2019), converts to ~740

595 metric ktons CO_2, equivalent to only approximately one month's worth of CO_2 derived from
596 depth at the total current diffuse emission rate for all of the Yellowstone Plateau Volcanic Field
597 (24 ± 12 kilotons CO_2 per day; Rahilly and Fischer, 2021). Inasmuch as the amount of CO_2
598 represented by the volume of travertine deposits studied here is spread out over time and space,
599 the amount is even more negligible compared with the present-day flux.

600 Although it could be a result of preservation bias, the apparently smaller volume of North
601 Hillside and Firehole Lake travertines suggests that late-Holocene wet periods either less
602 extreme and shorter than earlier episodes, and/or that the supply of fresh reactive sediments was
603 much less than what was available in the millennia following deglaciation. Regional climate
604 proxies, especially Yellowstone Lake $\delta^{18}O_{diatom}$, indicate that regional climate from ~6–4 ka was
605 highly variable with more frequent, short duration fluctuations between wet and dry conditions
606 (Brown et al., 2021; Fig. 7E). This provides evidence that smaller late-Holocene travertine
607 deposits may indeed be a result of shorter and less extreme climate events.

608 The absence of appreciable subsurface travertine deposits in research drill cores from the
609 Upper and Lower Geyser Basins suggests that large, buried travertine deposits on the scale
610 observed at Mammoth Hot Springs do not exist underneath the present-day silica-sinter deposits.
611 Hydrothermal travertine may have been deposited during or prior to the last glaciation and
612 during major magmatic shallow intrusions or eruptions; however, any evidence of such deposits
613 has been obliterated by recent large rhyolite flows (at 162, 111, and 70 ka; Christiansen, 2001;
614 Stelten et al., 2023) and glaciations at approximately 160–130 and 22–14.5 ka (Licciardi and
615 Pierce, 2018). Finally, within the Yellowstone caldera, the volume of travertine is not directly
616 proportional to the flux of CO_2 for two reasons. First, a significant amount of CO_2 discharge is
617 likely to occur through fumaroles and thermal features directly outgassing large amounts of CO_2

618 that have separated from deeper thermal fluids. Second, the occurrence and rate of travertine
619 deposition is not one mol $CaCO_3$ deposited to one mol of CO_2 degassed because this system is
620 not CO_2 limited; instead, it is typically limited by low calcium concentrations. Therefore, the
621 calculated CO_2 fluxes based on volumes of intra-caldera travertine are minimum estimates.
622 Nevertheless, the very small volumes of post-glacial age travertine within the Yellowstone
623 caldera does not suggest that there was a large postglacial surge in CO_2.

624 **CONCLUSION**

625 New ^{230}Th-U ages show that rare travertine deposits within the Yellowstone caldera
626 formed during three episodes that correspond with known wet climate periods. Travertine
627 deposition during wet climate increased the amount of meteoric water input into the shallow
628 hydrothermal system, which decreased reservoir water temperatures and subsurface boiling
629 while increasing the reactivity of thermal fluids with rock. These changes to the hydrothermal
630 system were buffered by the dissolution and precipitation of calcite deep within the system, so
631 calcium carbonate saturation upon discharge only occurred where hydrothermal waters were
632 coolest around the edges of main thermal basins and only for short periods (centuries to a few
633 millennia). The small volume of these deposits, especially the vanishingly small amount of
634 travertine with ages that closely postdate Pinedale glaciation, suggests no significant or sustained
635 surge in CO_2 during the early postglacial period; instead, late-Pleistocene and early-Holocene
636 travertine was primarily a result of an increased supply of calcium and magnesium associated
637 with high rates of chemical weathering of fresh glacial deposits. Late-Holocene travertine
638 deposition was catalyzed by the same mechanism, that is, sustained periods of increased
639 precipitation facilitated increased weathering and infiltration of labile elements, along with
640 decreasing the temperature of water-rock interactions in the periphery of the hydrothermal

system. The small volume of these deposits is consistent with the fact that late-Holocene wet periods were less extreme and shorter than earlier episodes. Hydrothermal travertine deposited within the Yellowstone caldera is a unique indicator of paleoclimatic, seismic, and hydrochemical variations over geologic time and provides insight into the evolution of one of the largest and most dynamic hydrothermal systems in the world.

ACKNOWLEDGMENTS

All samples were collected in cooperation with the National Park Service under research permits YELL-2019-SCI-8030, YELL-2020-SCI-8158, and YELL-2021-SCI-8192; we thank the NPS for their assistance with the permitting and sampling process. We acknowledge support from the U.S. Geological Survey Mendenhall Program to L. Harrison and NSF grant 2149482 to C. Whitlock. We would like to thank Annie Carlson, Mara Reed, Dakota Churchill, Mark Stelten, and Behnaz Houssini for their assistance with permitting and sample collection. We are grateful to journal reviews from two anomyous reviewers, U.S. Geological Survey reviews by Greg Pederson, Michael Clynne, L.P. Muffler, and Kevin Jones, constructive comments from associate editor Alessandro Zanazzi and efficient editorial handling by Bradley Singer. Any use of trade, firm, or product names is for descriptive purposes only and does not imply endorsement by the U.S. Government.

REFERENCES CITED

Allen, E.T., and Day, A.L., 1935, The hot springs of the Yellowstone National Park: Carnegie Inst. Washington Pub. 466, 525 p.

Bargar, K.E., 1978, Geology and thermal history of Mammoth hot springs, Yellowstone National Park, Wyoming: U.S. Geological Survey Bulletin 1444, p. 55, https://doi.org/10.3133/b1444.

Bargar, K.E., and Beeson, M.H., 1981, Hydrothermal alteration in research drill hole Y-2, Lower Geyser Basin, Yellowstone National Park, Wyoming: American Mineralogist, v. 66, p. 473–490.

Bargar, K.E., and Fournier, R.O., 1988. Effects of glacial ice on subsurface temperatures of hydrothermal systems in Yellowstone National Park, Wyoming: fluid-inclusion evidence: Geology, v. 16, p. 1077-1080.

Barth, A.M., Ceperley, E.G., Vavrus, C., Marcott, S.A., Shakun, J.D., and Caffee, M.W., 2022, ^{10}Be age control of glaciation in the Beartooth Mountains, USA from the latest Pleistocene through the Holocene: Geochronology Discussions, https://doi.org/10.5194/gchron-2022-17.

Bartlein, P.J., Anderson, P.M., Anderson, K.H., Edwards, M.E., Thompson, R.S., Webb, R.S., Webb, T. III, and Whitlock, C. 1998, Paleoclimate simulations for North America over the past 21,000 years: features of simulated climate and comparisons with paleoenvironmental data: Quaternary Science Reviews v. 17, p. 549–585, https://doi.org/10.1016/S0277- 3791(98)00012-2.

Berger, A.L., 1978, Long-Term Variations of Daily Insolation and Quaternary Climatic Changes: Journal of Atmospheric Sciences, v. 35, p. 2362–2367, https://doi.org/10.1175/1520-0469(1978)035<2362:LTVODI>2.0.CO;2.

Bergfeld, D., Lowenstern, J.B., Hunt, A.G., Shanks, P., and Evans, W.C., 2014, Gas and isotope chemistry of thermal features in Yellowstone National Park, Wyoming: USGS Scientific Investigations Report 2011–5012, 28 p., https://pubs.usgs.gov/sir/2011/5012/.

Bergfeld, D., Lowenstern, J.B., Hunt, A.G., Hurwitz, S., McCleskey, B.R., and Peek, S.E., 2019, Chemical and isotopic data on gases and waters for thermal and non-thermal features

across Yellowstone National Park (ver. 2.0, March 2019): U.S. Geological Survey Data Release, https://doi.org/10.5066/F7H13105.

Bindeman, I.N., and Lowenstern, J.B., 2016, Low δD hydration rinds in Yellowstone perlites record rapid syneruptive hydration during glacial and interglacial conditions: Contributions to Mineralogy & Petrology, v. 171(89), 24 p., http://dx.doi.org/10.1007/s00410-016- 1293-1.

Bischoff, J.L., and Rosenbauer, R.L., 1996, The alteration of rhyolite in CO_2 charged water at 200 and 350°C: The unreactivity of CO_2 at higher temperature: Geochemica et Cosmochimica Acta, v. 60(20), p. 3859–3867, https://doi.org/10.1016/0016-7037(96)00208-6.

Brown, S.R., Cartier, R., Schiller, C.M., Zahajská, P., Fritz, S.C., Morgan, L.A., Whitlock, C., Conley, D.J., Lacey, J.H., Leng, M.J., and Shanks, W.C., 2021, Multi-proxy record of Holocene paleoenvironmental conditions from Yellowstone Lake, Wyoming, USA: Quaternary Science Reviews, v. 274, 107275, https://doi.org/10.1016/j.quascirev.2021.107275

Capezzuoli, E., Gandin, A., and Pedley, M., 2014, Decoding tufa and travertine (fresh water carbonates) in the sedimentary record: The state of the art: Sedimentology, v. 61, p. 1–21, https://doi.org/10.1111/sed.12075.

Chafetz, H.S., and Guidry, S.A., 2003, Deposition and diagenesis of Mammoth Hot Springs Travertine, Yellowstone National Park, Wyoming, USA: Canadian Journal of Earth Science, v. 40, p. 1515–1529, https://doi.org/10.1139/e03-051.

Chafetz, H.S., and Lawrence, J.R., 1994, Stable isotopic variability within modern travertines: Géographie physique et Quaternaire, v. 48, p. 257–273, https://doi.org/10.7202/033007ar.

Cheng, H., Zhang, H., Spötl, C., Baker, J., Sinha, A., Li, H., Batolomé, M., Moreno, A., Kathayat, G., Zhao, J., Dong, X., Li, Y., Ning, Y., Jia, X., Zong, B., Brahim, Y.A., Pérez-Mejías, C., Cai, Y., Novello, V.F., Cruz, F.W., Severinghaus, J.P., An, Z., and Edwards, R.L., 2020, Timing and structure of the Younger Dryas event and its underlying climate dynamics: Proceedings of the National Academy of Science, v. 117(38), p. 23408–23417, https://doi.org/10.1073/pnas.2007869117.

Christiansen, R.L., 2001. The Quaternary and Pliocene Yellowstone Plateau Volcanic Field of Wyoming, Idaho, and Montana: U.S. Geological Survey Professional Paper 729-G, 145 p., https://pubs.usgs.gov/pp/pp729g/.

Chellman, N.J., Pederson, G.T., Lee, C.M., McWethy, D.B., Puseman, K., Stone, J.R., Brown, S.R., and McConnell, J.R., 2021, High elevation ice patch documents Holocene climate variability in the northern Rocky Mountains: Quaternary Science Advances, v. 3, 100021, https://doi.org/10.1016/j.qsa.2020.100021.

Coplen, T. B., 1994, Reporting of Stable Hydrogen, Carbon, and Oxygen Isotopic Abundances: Pure and Applied Chemistry, v. 66, p. 273–276. https://doi.org/10.1016/0375-6505(95)00024-0.

Cullen, J.T., Hurwitz, S., Barnes, J.D., Lassiter, J.C., Penniston-Dorland, S., Kasemann, S.A., and Thordsen, J.J., 2019, Temperature-dependent variations in mineralogy, major element chemistry and the stable isotopes of boron, lithium, and chlorine resulting from hydration of rhyolite: Constraints from hydrothermal experiments at 150 to 350°C and 25 MPa: Geochemica et Cosmochimica Acta, v. 261, p. 269–287, https://doi.org/10.1016/j.gca.2019.07.012.

Dahms, D., Egli, M., Fabel, D., Harbor, J., Brandová, D., de Castro Portes, R., and Christl, M., 2018, Revised Quaternary glacial succession and post-LGB recession, southern Wind River Range, Wyoming, USA: Quaternary Science Reviews, v. 192, p. 167–184, https://doi.org/10.1016/j.quascirev.2018.05.020.

De Boever, E., Jaramillo-Vogel, D., Bouvier, A.-S., Frank, N., Schröder-Ritzrau, A., Baumgarter, L., Swennen, R., and Foubert, A., 2021, The fate of a travertine record: Impact of early diagenesis on the Y-10 core (Mammoth Hot Springs, Yellowstone National Park, USA): Depositional Record, v. 8, p. 220–250, https://doi.org/10.1002/dep2.143.

Finn, C., Bedrosian, P.A., Holbrook, W.S., Auken, E., Bloss, B.R., and Crosbie, J., 2022, Geophysical imaging of the Yellowstone hydrothermal plumbing system: Nature, v. 603, p. 643–647, https://doi.org/10.1038/s41586-021-04379-1.

Fouke, B.W., Farmer, J.D., Des Marias, D.J., Pratt, L., Sturchio, N.C., Burns, P.C., and Discipulo, M.K., 2000, Depositional facies and aqueous-solid geochemistry of the travertine-depositing hot springs (Angel Terrace, Mammoth Hot Springs, Yellowstone National Park, U.S.A.: Journal of Sedimentary Research, v. 70(3), p. 565–585, https://doi.org/10.1306/2DC40929-0E47-11D7-8643000102C1865D.

Fouke, B.W., 2011. Hot-spring Systems Geobiology: abiotic and biotic influences on travertine formation at Mammoth Hot Springs, Yellowstone National Park, USA: Sedimentology, v. 58, p. 170–219, https://doi.org/10.1111/j.1365- 3091.2010.01209.x.

Fournier, R.O., 1989. Geochemistry and dynamics of the Yellowstone National Park hydrothermal system: Annual Reviews in Earth and Planetary Science, v. 17, p. 13–53. https://doi.org/10.1146/annurev.ea.17.050189.000305

Friedman, I., 1970, Some investigations of the deposition of travertine from Hot Springs—I. The isotopic chemistry of a travertine-depositing spring: Geochemica et Cosmochimica Acta, v. 34, p. 1303–1315, https://doi.org/10.1016/0016-7037(70)90043-8.

Gosse, J.C., Evenson, E.B., Klein, J., Lawn, B., and Middleton, R., 1995, Precise cosmogenic 10Be measurements in western North America: Support for a global Younger Dryas cooling event: Geology, v. 23(10), p. 877–880, https://doi.org/10.1130/0091-7613(1995)023%3C0877:PCBMIW%3E2.3.CO;2.

Harrison, L.N., Hurwitz, S., Paces, J.B., McCleskey, R.B., Roth, D.A., Conrey, R., and Stelten, M.E., 2022, Elemental and Strontium Isotopic Composition of Select Central Plateau and Upper Basin Member Rhyolites, Yellowstone Plateau Volcanic Field: U.S. Geological Survey Data Release, https://doi.org/10.5066/P952ZE74.

Harrison, L.N., Hurwitz, S., Paces, J.B., and Peek, S., 2023, Radiogenic Sr isotope composition ($^{87}Sr/^{86}Sr$), stable oxygen and carbon isotope composition, elemental concentrations, and U-Th disequilibrium ages for travertine deposits from various locations in Yellowstone National Park: U.S. Geological Survey Data Release, https://doi.org/10.5066/P9G2R6ZF.

Hildreth, W., Halliday, A.N., and Christiansen, R.L., 1991, Isotopic and chemical evidence concerning the genesis and contamination of basaltic and rhyolitic magma beneath the Yellowstone Plateau Volcanic Field: Journal of Petrology, v. 32(1), p. 63–138, https://doi.org/10.1093/petrology/32.1.63.

Hurwitz, S., and Lowenstern, J.B., 2014, Dynamics of the Yellowstone hydrothermal system: Reviews of Geophysics, v. 52, p. 375-411, https://doi.org/10.1002/2014RG000452.

Hurwitz, S., Evans, W.C., and Lowenstern, J.B., 2010, River solute fluxes reflecting active hydrothermal chemical weathering of the Yellowstone Plateau Volcanic Field, USA:

Chemical Geology, v. 276(3-4), p. 331–343, https://doi.org/10.1016/j.chemgeo.2010.07.001.

Kampman, N., Burnside, N.M., Shipton, Z.K., Chapman, H.J., Nicholl, J.A., Ellam, R.M., and Bickle, M.J., 2012, Pulses of carbon dioxide emissions from intracrustal faults following climatic warming: Nature Geoscience, v. 5, p. 352–358, https://doi.org/10.1038/ngeo1451.

Kele, S., Breitenbach, S.F.M., Capezzuoli, E., Meckler, A.N., Ziegler, M., Millan, I.M., Kluge, T., Deák, J., Hanselmann, K., John, C.M., Yan, H., Liu, Z., and Bernasconi, S.M., 2015, Temperature dependence of oxygen- and clumped isotope fractionation in carbonates: A study of travertines and tufas in the 6–95°C temperature range: Geochimica et Cosmochimica Acta, v. 168, p. 172–192, http://dx.doi.org/10.1016/j.gca.2015.06.032.

Kharaka, Y.K., Mariner, R.H., Bullen, T.D., Kennedy, B.M., and Sturchio, N.C., 1991, Geochemical investigations of hydraulic connections between Corwin Springs Known Geothermal Area and adjacent parts of Yellowstone National Park, *in* Sorey, M., ed., Effects of Potential Geothermal Development in the Corwin Springs Known Geothermal Resources Area, Montana, on the Thermal Features of Yellowstone National Park: U.S. Geological Survey Water-Resources Investigations Report 91-4052, p. F1–F38.

Kharaka, Y.K., Thordsen, J.L., and White, L.D., 2002. Isotope and chemical compositions of meteoric and thermal waters and snow from the greater Yellowstone National Park region: U.S. Geological Survery Open-File Report 2002-194, 75 p. https://doi.org/10.3133/ofr02194.

799 Keith, T.E.C., and Muffler, L.J.P., 1978, Minerals produced during cooling and hydrothermal
800 alteration of ash flow tuff from Yellowstone drill hole Y-5: Journal of Volcanology and
801 Geothermal Research, v. 3, p, 373–402, https://doi.org/10.1016/0377-0273(78)90044-6.
802 Kohn, M.J., and McKay M., 2010, Stable isotopes of fossil teeth corroborate key general
803 circulation model predictions for the Last Glacial Maximum in North America:
804 Geophysical Research Letters, v. 37, L22702, https://doi.org/10.1029/2010GL045404.
805 Krause, T.R., and Whitlock, C., 2013, Climate and vegetation change during the late-
806 glacial/early-Holocene transition inferred from multiple proxy records from Blacktail
807 Pond, Yellowstone National Park, USA: Quaternary Research, v., 79(3), p. 391–402,
808 https://doi.org/10.1016/j.yqres.2013.01.005.
809 Krause, T.R., and Whitlock, C., 2017, Climatic and non-climatic controls shaping early
810 postglacial conifer history in the norther Greater Yellowstone Ecosystem, USA: Journal
811 of Quaternary Science, v. 32(7), p. 1022–1036, https://doi.org/10.1002/jqs.2973.
812 Larson, D.J., Crump, S.E., and Blumm, A., 2020, Alpine glacier resilience and Neoglacial
813 fluctuations linked to Holocene snowfall trends in the western United States: Science
814 Advances, v. 6, eabc7661, https://doi.org/10.1126/sciadv.abc7661.
815 Licciardi, J.M., and Pierce, K.L., 2018, History and dynamics of the Greater Yellowstone Glacial
816 System during the last two glaciations: Quaternary Science Reviews, v. 200, p. 1–33,
817 https://doi.org/10.1016/j.quascirev.2018.08.027.
818 Loewen, M.W., Bindeman, I.N., and Melnik, O.E. 2017, Eruption mechanisms and short
819 duration of large rhyolitic lava flows of Yellowstone: Earth and Planetary Science
820 Letters, v. 458, p. 80–91, https://doi.org/10.1016/j.epsl.2016.10.034.

821 Lowenstern, J.B., Evans, W.C., and Bergfeld, D., 2005, Diffuse and direct sources of CO_2 from
822 Terrace Spring, a large-volume travertine-forming spring at Yellowstone National Park:
823 Palermo, Italy, 9th Workshop of the IAVCEI Commission on the Chemistry of Volcanic
824 Gasses, Abstract, http://dx.doi.org/10.13140/RG.2.1.1675.3681
825 Lowenstern, J.B., Bergfeld, D., Evans, W.C., and Hunt, A.G., 2015, Origins of geothermal
826 gasses at Yellowstone: Journal of Volcanology and Geothermal Research, v. 302, p. 87–
827 101, https://doi.org/10.1016/j.jvolgeores.2015.06.010.
828 Ludwig, K.R., and Paces, J.B., 2002, Uranium-series dating of pedogenic silica and carbonate,
829 Crater Flat, Nevada: Geochimica et Cosmochimica Acta, v. 66(3), p. 487–506,
830 https://doi.org/10.1016/S0016-7037(01)00786.
831 Lundeen, Z. Brunelle, A., Burns. S.J., Polyak, V., and Asmerom, Y., 2013, A speleothem record
832 of Holocene paleoclimate from the northern Wasatch Mountains, southeast Idaho, USA:
833 Quaternary International, v. 310, p. 83-95, https://doi.org/10.1016/j.quaint.2013.03.018.
834 Luo, L., Capezzuoli, E., Rogerson, M., Vaselli, O., Wen, H., and Lu, Z., 2022, Precipitation of
835 carbonate minerals in travertine-depositing hot springs: Driving forces,
836 microenvironments, and mechanisms: Sedimentary Geology, v. 438, 106207,
837 https://doi.org/10.1016/j.sedgeo.2022.106207.
838 Mancini, A., Frondini, F., Capezzuoli, E., Mejia, E.G., Lezzi, G., Matarazzi, D., Brogi, A., and
839 Swennen, R., 2019, Evaluating the geogenic CO_2 flux from geothermal areas by
840 analyzing Quaternary travertine masses. New data from western central Italy and review
841 of previous CO_2 flux data: Quaternary Science Reviews, v. 215, p. 132–143,
842 https://doi.org/10.1016/j.quascirev.2019.04.030.

Marcott, S.A., Clark, P.U., Shakun, J.D., Brook, E.J., Davis, P.T., and Caffee, M.W., 2019, ^{10}Be age constraints on latest Pleistocene and Holocene cirque glaciation across the western United States: NPJ Climate and Atmospheric Science, v. 5, https://doi.org/10.1038/s41612-019-0062-z.

McCleskey, R.B., Roth, D.A., Nordstrom, D.K., Hurwitz, S., Holloway, J.M., Bliznik, P.A., Ball, J.W., Repert, D.A., and Hunt, A.G., 2022, Water-Chemistry and Isotope Data for Selected Springs, Geysers, Streams, and Rivers in Yellowstone National Park, Wyoming: U.S. Geological Survey data release, https://doi.org/10.5066/P92XKJU7.

McKenzie, W.F., and Truesdell, A.H., 1977, Geothermal reservoir temperatures estimated from the oxygen isotope compositions of dissolved sulfate and water from hot springs and shallow drillholes: Geothermics, v. 5, p. 51–61, https://doi.org/10.1016/0375-6505(77)90008-6.

Moran, J.J., Whitmore, L.M., Jay, Z.J., Jennings, R., Beam, J.P., Kreuzer, H.W., and Inskeep, W.P., 2017, Dual stable isotope of CH_4 from Yellowstone hot-springs suggests hydrothermal processes involving magmatic CO_2: Journal of Volcanology and Geothermal Research, v. 341, p. 187–192, https://doi.org/10.1016/j.jvolgeores.2017.05.011.

Morgan, L.A., Shanks, W.C.P., Pierce, K.L., Iverson, N., Schiller, C.M., Brown, S.R., Zahajska, P., Cartier, R., Cash, R.W., Best, J.L., Whitlock, C., Fritz, S., Benzel, W., Lower Geyser Basins, H., Lovalo, D.A., and Licciardi, J.M., 2022, The dynamic floor of Yellowstone Lake, Wyoming, USA: The last 14 k.y. of hydrothermal explosions, venting, doming, and faulting: GSA Bulletin, v. 135, https://doi.org/10.1130/B36190.1.

Muffler, L.J.P., White, D.E., Truesdell, A.H., and Fournier, R.O., 1982a, Geologic map of Lower Geyser Basin, Yellowstone National Park, Wyoming: U.S. Geological Survey Miscellaneous Investigations Series Map I-1373, scale 1:2400, https://doi.org/10.3133/i1373.

Muffler, L.J.P., White, D.E., Beeson, M.H., and Truesdell, A.H., 1982b, Geologic map of Upper Geyser Basin, Yellowstone National Park, Wyoming: U.S. Geological Survey Miscellaneous Investigations Series Map I-1371, scale 1:2400, https://doi.org/10.3133/i1371.

Paces, J.B., Hurwitz, S., Harrison, L.N., and Cullen, J.T., 2022, Sr and U concentrations and radiogenic isotope compositions ($^{87}Sr/^{86}Sr$, $^{234}U/^{238}U$) of thermal waters, streamflow, travertine, and rock samples along with U-Th disequilibrium ages for travertine deposits from various locations in Yellowstone National Park, USA: U.S. Geological Survey data release, https://doi.org/10.5066/P9JPX2RO.

Pierce, K.L., Muhs, D.R., Fosberg, M.A., Mahan, S.A., Rosenbaum, J.G., Licciardi, J.M., and Pavich, M.J., 2011, A loess-paleosol record of climate and glacial history over the past two glacial-interglacial cycles (~150 ka), southern Jackson Hole, Wyoming: Quaternary Research, v. 76, p. 119–141, https://doi.org/10.1016/j.yqres.2011.03.006.

Pierce, K.L., Adams, K.D., and Sturchio, N.C., 1991, Geologic Setting of the Corwin Springs Known Geothermal Resources Area-Mammoth Hot Springs Area in and adjacent to Yellowstone National Park, *in* Sorey, M., ed., Effects of Potential Geothermal Development in the Corwin Springs Known Geothermal Resources Area, Montana, on the Thermal Features of Yellowstone National Park: v. 91, https://doi.org/10.3133/wri914052.

888 Priewisch, A., Crossey, L.J., Karlstrom, K.E., Polyak, V.J., Asmerom, Y., Nereson, A., and
889 Ricketts, J.W., 2014, U-series geochronology of large-volume Quaternary travertine
890 deposits of the southeastern Colorado Plateau: Evaluating episodicity and tectonic and
891 paleohydrologic controls: Geosphere, v. 10(2), p. 401–423,
892 https://doi.org/10.1130/GES00946.1.
893 Rahilly, K.E., and Fischer, T.P., 2021, Total diffuse CO_2 flux from Yellowstone caldera
894 incorporating high CO_2 emissions from cold degassing sites: Journal of Volcanological
895 and Geothermal Research, v. 419, 107383,
896 https://doi.org/10.1016/j.jvolgeores.2021.107383.
897 Rye, R.O., and Truesdell, A.H., 2007, The question of recharge to the deep thermal reservoir
898 underlying the geysers and hot springs of Yellowstone National Park *in* Morgan, L.A.,
899 ed., Integrated Geoscience Studies int he Greater Yellowstone Area-- Volcanic, Tectonic,
900 and Hydrothermal Processes in the Yellowstone Geoecosystem: U.S. Geological Survey
901 Professional Paper 1717, p. 239–270, https://doi.org/10.3133/pp1717H.
902 Schiller, C.S., Whitlock, C., and Brown, S., 2021, Holocene geo-ecological evolution of Lower
903 Geyser Basin, Yellowstone National Park (USA): Quaternary Research, p. 1–17,
904 https://doi.org/10.1017/qua.2021.42.
905 Shuman, B.N., and Marsicek, J.P., 2016, The Structure of Holocene Climate Change in Mid-
906 Latitude North America: Quaternary Science Reviews, v. 141, p. 38–51,
907 https://doi.org/10.1016/j.quascirev.2016.03.009.
908 Shuman, B.N., and Serravezza, M., 2017, Patterns of hydroclimatic change in the Rocky
909 Mountains and surrounding regions since the last glacial maximum: Quaternary Science
910 Reviews, v. 17, p. 58–77, https://doi.org/10.1016/j.quascirev.2017.08.012.

911 Stelten, M.E., Thomas, N., Pivarunas, A., and Champion, D., 2023. Spatio-temporal clustering of
912 post-caldera eruptions at Yellowstone caldera: implications for volcanic hazards and pre-
913 eruptive magma reservoir configuration: Bulletin of Volcanology, v. 85(55),
914 https://doi.org/ 10.1007/s00445-023-01665-w.
915 Sturchio, N.C., Keith, T.E.C., and Muehlenbachs, K., 1990, Oxygen and carbon isotope ratios of
916 hydrothermal minerals from Yellowstone drill cores: Journal of Volcanology and
917 Geothermal Research, v. 40, p. 23–37, https://doi.org/10.1016/0377- 0273(90)90104-N.
918 Sturchio, N.C., Pierce, K.L., Murrell, M.T., and Sorey, M.L., 1994, Uranium-Series ages of
919 travertines and timing of the last glaciation in the Northern Yellowstone area, Wyoming-
920 Montana: Quaternary Research, v. 41(3), p. 265–277,
921 https://doi.org/10.1006/qres.1994.1030.
922 Uysal, I.T., Feng, Y., Zhao, J.-X., Isik, V., Nuriel, P., and Golding, S.D., 2009, Hydrothermal
923 CO_2 degassing in seismically active zones during the Late Quaternary: Chemical
924 Geology, v. 265, p. 442–454, https://doi.org/10.1016/j.quascirev.2019.04.029.
925 Vazquez, J.A., and Reid, M.R., 2002, Time scales of magma storage and differentiation of
926 voluminous high-silica rhyolites at Yellowstone caldera, Wyoming: Contributions to
927 Mineralogy Petrology, v. 144, p. 274–285, https://doi.org/10.1007/s00410-002-0400-7.
928 Waldrop, H.A. 1975, Surficial geologic map of the Old Faithful quadrangle, Yellowstone
929 National Park, Wyoming: Miscellaneous Investigations Series Map I-649,
930 https://ngmdb.usgs.gov/Prodesc/proddesc_9427.htm.
931 Waldrop, H.A., and Pierce, K.L., 1975, Surficial geologic map of the Madison junction
932 quadrangle Yellowstone National Park, Wyoming: Miscellaneous Investigation Series
933 Map I-651, https://ngmdb.usgs.gov/Prodesc/proddesc_9429.htm.

Wang, P., Du, Y., Yu, W., Algeo, T.J., Zhou, Q., Xu, Y., Qi, L., Yuan, L., and Pan, W., 2020, The chemical index of alteration (CIA) as a proxy for climate change during glacial-interglacial transitions in Earth history: Earth-Science Reviews, v. 201, 103032, https://doi.org/10.1016/j.earscirev.2019.103032.

Watts, K.E., Bindeman, I.N., and Schmitt, A.K., 2012, Crystal scale anatomy of a dying supervolcano: an isotope and geochronology study of individual phenocrysts from voluminous rhyolites of the Yellowstone caldera: Contributions to Mineralogy Petrology, v. 164, p. 45–67, https://doi.org/10.1007/s00410-012-0724-x.

Werner, C., and Brantley, S., 2003, CO_2 emissions from the Yellowstone volcanic system: Geochemistry Geophysics Geosystems, v. 4(7), 1061, https://doi.org/10.1029/2002GC000473.

White, D.E., Fournier, R.O., Muffler, L.P.J., and Truesdell, A.H., 1975, Physical results of research drilling in thermal areas of Yellowstone National Park, Wyoming: U.S. Geological Survey Professional Paper 892, 70 p.

Whitlock, C., 1993, Postglacial vegetation and climate of Grand Teton and southern Yellowstone National Parks: Ecological Monographs, v. 63, p. 173–198, https://doi.org/10.2307/2937179.

Whitlock, C., Dean, W.E., Fritz, S.C., Stevens, L.R., Stone, J.R., Power, M.J., Rosenbaum, J.R., Pierce, K.L., and Bracht-Flyr, B. 2012, Holocene seasonal variability inferred from multiple proxy records from Crevice Lake, Yellowstone National Park, USA: Paleogeography, Paleoclimatology, Paleoecology, v. 331–332, p. 90–103, https://doi.org/10.1016/j.palaeo.2012.03.001.

Whitlock, C., Dean, W., Rosenbaum, J., Stevens, L., Fritz, S., Bracht, B., and Power, M., 2008, A 2650-year-long record of environmental change from northern Yellowstone National Park based on a comparison of multiple proxy data: Quaternary International, v. 188, p. 126–138, https://doi.org/10.1016/j.quaint.2007.06.005.

FIGURE CAPTIONS

Figure 1. A) Map of the location of travertine deposits within Yellowstone National Park (the black dashed line is the boundary of Yellowstone National Park). Open circles labeled with large font indicate intra-caldera travertine deposits investigated in this study. Filled circles labeled with small font indicate other travertine areas in Yellowstone National Park not included in this study. The green dotted outline indicates the most recent (~631 ka) caldera, and the orange lines denote the fault zone that delineates the Norris-Mammoth corridor. Panels B–D show lithostratigraphic units draped onto topography, the locations of travertine samples, and active hydrothermal features. Background on these figures is 2020 LiDAR data (U.S. Geological Survey, 20211222, USGS Original Project Resolution WY_YellowstoneNP_2020_D20: U.S. Geological Survey) and geologic contacts (Waldrop and Pierce, 1975; Muffler et al., 1982a, 1982b; Christiansen, 2001). B) Firehole Lake, Lower Geyser Basin. C) Hillside Springs Group, Upper Geyser Basin. D) Travertine near Morning Glory Pool, Upper Geyser Basin. See supplementary Figure 1 for a map of Terrace Spring, descriptions of travertine samples, and field photographs.

Figure 2. Cartoons illustrating different potential deposition mechanisms of within-caldera travertine discussed in the text. Blue arrows indicate cold meteoric infiltration while large dark

orange arrows indicate hot thermal water upflow zones and thin light orange arrows indicate lower temperature thermal waters with shallower flow paths than the main upflow zones. Note that the flux of deep CO_2 from the Yellowstone deep magmatic reservoir (approximately 5–17 km depth) is portrayed as constant from the late Pleistocene to the Present for all scenarios. A) Increased weathering of surficial sediments and recharge to the hydrothermal system during deglaciation or periods of high precipitation. The increased availability of fresh glacial tills composed of glacially transported rocks (basalts, andesites, and dacites) from the eastern Yellowstone region provided critical sources of Ca^{2+}, Mg^{2+}, and HCO_3^- to the hydrothermal system; the rates of weathering of these surficial sediments increases during periods of wet climatic conditions. B) release of accumulated volatiles (mostly CO_2) by earthquakes from previously hydrothermally sealed subsurface. Volatile release is highest in locations above large faults, like Terrace Spring which is located at the convergence of the Mammoth-Norris fault corridor and the 631 ka caldera rim fault. C) Off gassing of a magmatic intrusion (here illustrated as a shallow dike, <5 km depth) can result in large travertine deposits that are spatially constrained to locations above the dike intrusion; as there have been no known volcanic eruptions in the Yellowstone Plateau Volcanic Field since ~70 ka, we rule out this as a potential mechanism for the formation of within-caldera travertine.

Figure 3. Uranium-series (^{230}Th-U) ages for travertines. Blue fields designate relevant climatic events: the latest stage of Pinedale glaciation (Licciardi and Pierce, 2018), the Younger Dryas cold event (Cheng et al., 2020), and the cool climatic episode identified in Yellowstone Lake sediment cores (Brown et al., 2021). The histogram on the right side of the diagram is a kernel density estimate of U-series ages, illustrating periods of high travertine deposition. The ages and

errors for each travertine group discussed in text are shown on top of the diagram, where n is the number of travertine samples of that age (points on the plot denote different analytical aliquots, some of which are different travertine layers from the same sample).

Figure 4. Stable isotope composition of Yellowstone hydrothermal travertines and other materials. $\delta^{18}O$ (‰ VSMOW) and $\delta^{13}C$ (‰ VPDB) of A) Yellowstone hydrothermal travertines from this study compared to those from Mammoth Hot Springs and B) Yellowstone hydrothermal travertines and related reservoirs. Error bars are smaller than the data points on both plots (±0.2‰ for both $\delta^{18}O_{carbonate}$ and $\delta^{13}C_{carbonate}$). Data for Mammoth Hot Springs travertine are from Fouke et al. (2000), Friedman (1970), Chafetz and Lawrence (1994), De Boever et al. (2021), and Chafetz and Guidry (2003). The legend in panel (A) applies to the entire figure. In panel (B) the range of $\delta^{18}O_{water}$ for modern Yellowstone cold waters (light-blue vertical band) is from Kharaka et al. (2002). Compositions of individual water samples from the Hillside Springs Group and Mammoth Hot Springs are shown with asterisk symbols (data from McCleskey et al., 2022, Fouke et al., 2000, respectively). Yellowstone Plateau Volcanic Field $\delta^{13}C_{gas}$ values measured in fumarole gas by Bergfeld et al. (2019) are yellow circles used to define the yellow horizontal band. Values of $\delta^{18}O_{water}$ and $\delta^{13}C_{water}$ in thermal waters ($\delta^{13}C$ measured from dissolved inorganic carbon) are shown as orange circles and all plot within the fumarole band. Data for northern Yellowstone region sedimentary rocks (from Friedman (1970) and Kharaka et al. (1991)) include carbonate-bearing limestones and evaporites of the Madison Formation and are shown as gray diamonds within a light-green box. For comparison, the range of $\delta^{18}O_{seawater}$ in Mississippian seawater is shown as a vertical gray band. Simple isotopic mixing between average Paleozoic and Mesozoic sedimentary rocks (exposed and sampled north of

Yellowstone National Park; Friedman, 1970) ($\delta^{18}O_{av\ sed} \approx +21‰$ and $\delta^{13}C_{av\ sed} \approx -0.6$ ‰), and average magmatic gas as approximated by fumarole compositions ($\delta^{18}O_{av\ gas} \approx -21‰$ and $\delta^{13}C_{av\ gas} \approx -3‰$),) is shown by the gray line with tick marks at 10% intervals (average values of end-members used in the calculation are shown with star symbols). Subsurface boiling will drive thermal fluids to the right on the diagram (dashed boiling line) whereas rapid kinetic fractionation with subaerial CO_2 degassing will drive waters vertically on the diagram (CO_2 degassing dashed line). It is possible that the within-caldera travertines are formed by mixing between magmatic CO_2 and dissolution of Paleozoic and Mesozoic sedimentary rocks in the subsurface followed by rapid CO_2 degassing, or thermal water boiling followed by rapid CO_2 degassing, or a combination of the two. C) Shows the range of $\delta^{18}O_{water}$ calculated to be in equilibrium with the measured $\delta^{18}O_{carbonate}$ at 70°C and 80°C (using the equation of Kele et al., 2015). Values falling below the mean $\delta^{18}O_{water}$ for modern thermal waters (dashed horizontal line) illustrate that sources of late Pleistocene and early Holocene groundwater had lower $\delta^{18}O_{water}$, consistent with glacial meltwater and cool climate precipitation recharging aquifers during that time. D) The calculated $\delta^{18}O_{waters}$ at 80°C from panel (C) are plotted along the global meteoric water line (GMWL) illustrating the likely predicted oxygen and deuterium values of recharge waters into the hydrothermal system at the time of different travertine deposition. Compositions of modern Yellowstone cold waters are plotted for context (data from Rye and Truesdell, 2007) and outlined in the blue shaded field.

Figure 5. Chemical compositions of Yellowstone intra-caldera travertines plotted against their ^{230}Th-U age. A) Ca/(Mg+Ca). B) CIA (chemical index of alteration) calculated as CIA = $[Al_2O_3/(Al_2O_3 + CaO^* + Na_2O + K_2O)] \times 100$ where all oxides are calculated as molar oxides

and CaO* is calcium oxide in the silicate fraction only, here calculated using CaO = Na_2O. The blue field designates the latest stage of Pinedale glaciation, and the gray field designates the Younger Dryas cold event (Cheng et al., 2020).

Figure 6. Present-day measured strontium isotope composition (not age corrected) of travertines, aquifer rocks, and groundwaters plotted by longitude. A) shows travertine data relative to modern groundwaters discharging in Upper and Lower Geyser Basins and the rocks underlying or adjacent to those basins. The upper and lower bounds for each rhyolite or tuff unit are given as horizontal lines that represent the range of measured $^{87}Sr/^{86}Sr$ for those units. The horizontal gray-purple band is the range of the Middle and South Biscuit Basin flows, and the horizontal gray band is the combined range of $^{87}Sr/^{86}Sr$ observed in Lava Creek Tuff member B, West Yellowstone flow, Mallard Lake flow, Summit Lake flow, Elephant Back flow, and Nez Perce flow. B) Enlarged version of travertine data and the ranges of $^{87}Sr/^{86}Sr$ for the latter group of flows. Water data are from Paces et al. (2022). Yellowstone rock data are from Paces et al. (2022), Harrison et al. (2022), Vazquez and Reid (2002), Watts et al. (2012); and Hildreth et al. (1991). Error bars (95% confidence) are smaller than the points.

Figure 7. Travertine $\delta^{18}O_{carbonate}$ and age probability density curve (I, bottom) plotted with regional and local paleoclimate indicators. The vertical gray bands indicate time periods of Yellowstone intra-caldera travertine deposition. A) Summer insolation anomaly (in watts per square meter) at 44.5°N (Berger, 1978). B) Cosmogenic exposure probability density functions of moraine ages in the Yellowstone region (Licciardi and Pierce, 2018; Purple curve = Lake Solitude, Teton County, WY; Red curve = Inner Jenny Lake, Teton County, WY; Yellow curve

= Pinedale 2, Teton County, WY; Orange curve = Outer Jenny Lake, Teton County, WY; Magenta curve = Junction Butte, Northern YNP). C) Modeled composite *Picea* abundance in the Yellowstone region (*P. engelmannii* was among the first conifers to colonize the deglaciated landscape, as it is frost tolerant and can endure long cold winters and short cool summers; Krause and Whitlock, 2017). D) Composite lake-level history based on percent of lakes located within the U.S. Rocky Mountains that were >0.5 standard deviations below their mean level per 250-year interval (Shuman and Serravezza, 2017). E) Yellowstone Lake $\delta^{18}O_{diatom}$ measured in fossil diatoms from lake sediment cores (Brown et al., 2021). F) Goose Lake ratio of arboreal pollen to non-arboreal pollen (AP:NAP), an indication of the local forest density (Schiller et al., 2021). G) Goose Lake hydrothermal history based on arsenic concentration in sediment cores; higher arsenic concentrations indicate a higher input of hydrothermal water (Schiller et al., 2021). H) Beartooth ice patch net ice accretion rate in cm yr^{-1}, lower ice accretion indicates warmer temperatures and less winter precipitation (Chellman et al., 2021).

[1]Supplemental Material. *[Field Photos for all travertine deposits described in this manuscript and a geologic map of Terrace Spring]* Please visit https://doi.org/10.1130/XXXX to access the supplemental material, and contact editing@geosociety.org with any questions.

Figure 1

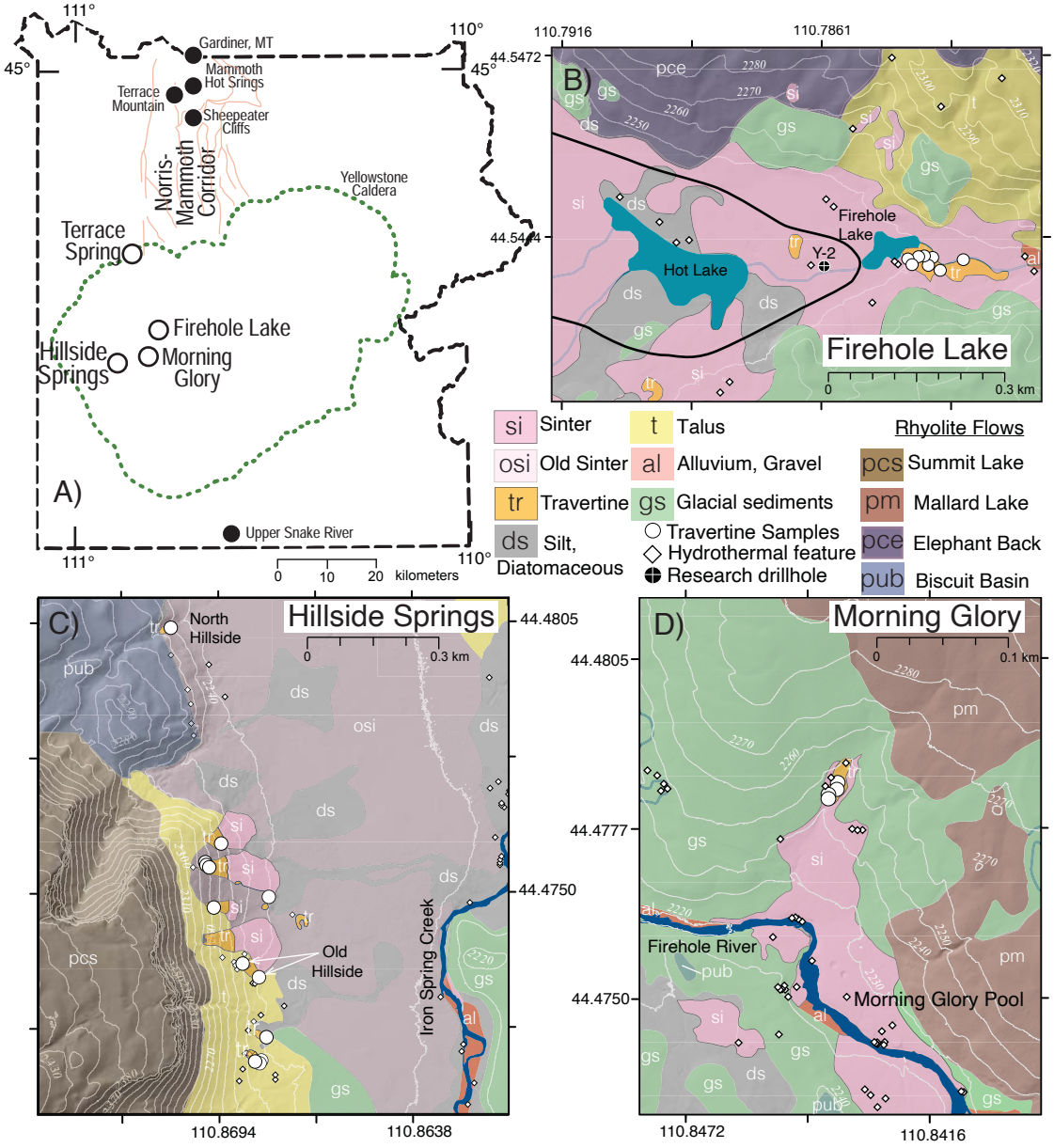
A)
111°
110°
45°
Gardiner, MT
Mammoth Hot Srings
Terrace Mountain
Sheepeater Cliffs
Norris-Mammoth Corridor
Yellowstone Caldera
Terrace Spring
Firehole Lake
Hillside Springs
Morning Glory
Upper Snake River
0 10 20 kilometers
B)
110.7916
110.7861
44.5472
44.5444
Firehole Lake
Hot Lake
Y-2
0 0.3 km
si Sinter
osi Old Sinter
tr Travertine
ds Silt, Diatomaceous
t Talus
al Alluvium, Gravel
gs Glacial sediments
Travertine Samples
Hydrothermal feature
Research drillhole
Rhyolite Flows
pcs Summit Lake
pm Mallard Lake
pce Elephant Back
pub Biscuit Basin
C)
Hillside Springs
North Hillside
Old Hillside
Iron Spring Creek
0 0.3 km
44.4805
44.4750
110.8694
110.8638
D)
Morning Glory
Firehole River
Morning Glory Pool
0 0.1 km
44.4805
44.4777
44.4750
110.8472
110.8416

Figure 2

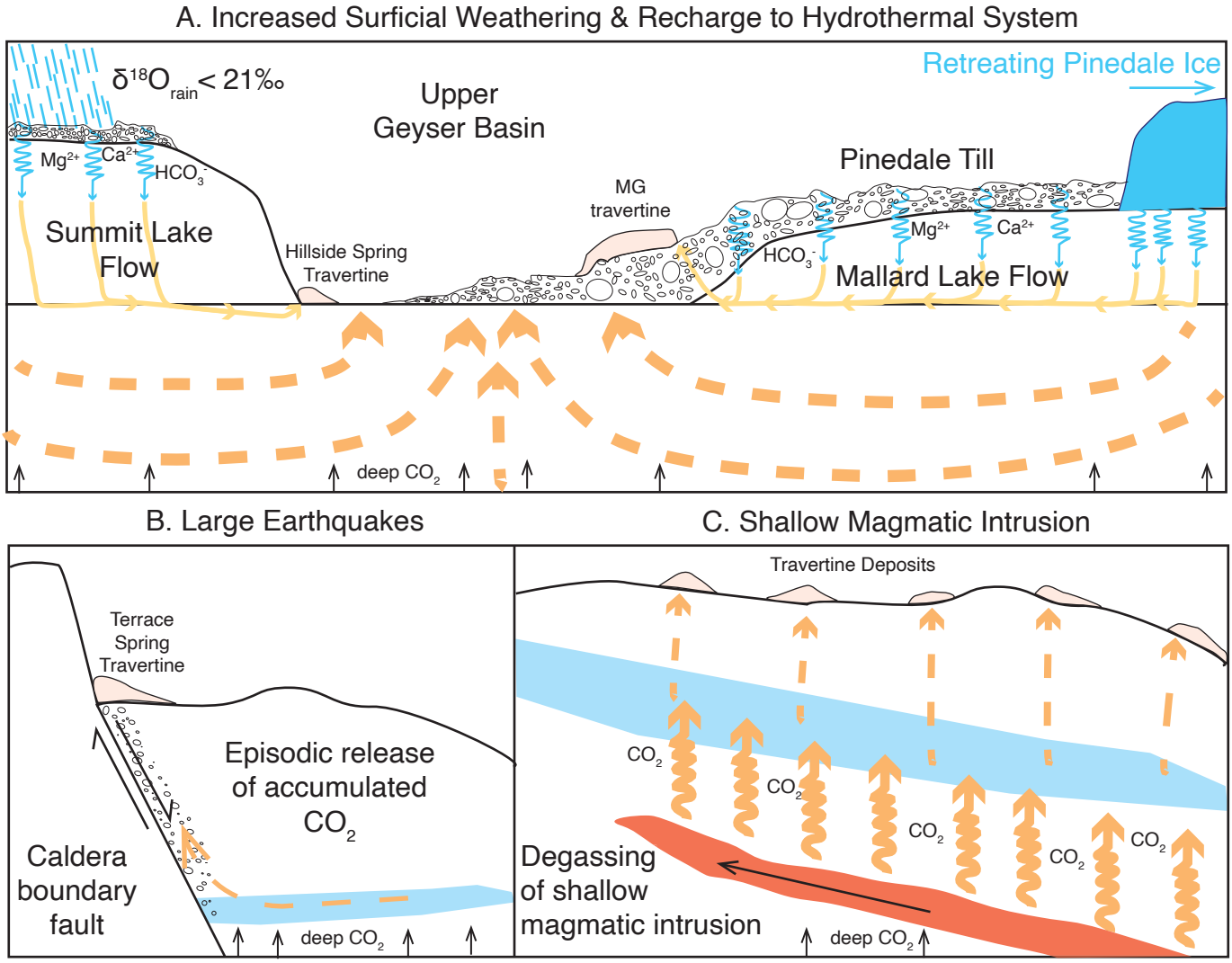
A. Increased Surficial Weathering & Recharge to Hydrothermal System
δ18Orain < 21‰
Upper
Geyser Basin
Retreating Pinedale Ice
Mg2+
Ca2+
HCO3-
Summit Lake
Flow
Hillside Spring
Travertine
MG
travertine
Pinedale Till
Mg2+
Ca2+
HCO3-
Mallard Lake Flow
deep CO2
B. Large Earthquakes
Terrace
Spring
Travertine
Episodic release
of accumulated
CO2
Caldera
boundary
fault
deep CO2
C. Shallow Magmatic Intrusion
Travertine Deposits
CO2
CO2
CO2
CO2
CO2
Degassing
of shallow
magmatic intrusion
deep CO2

Figure 3

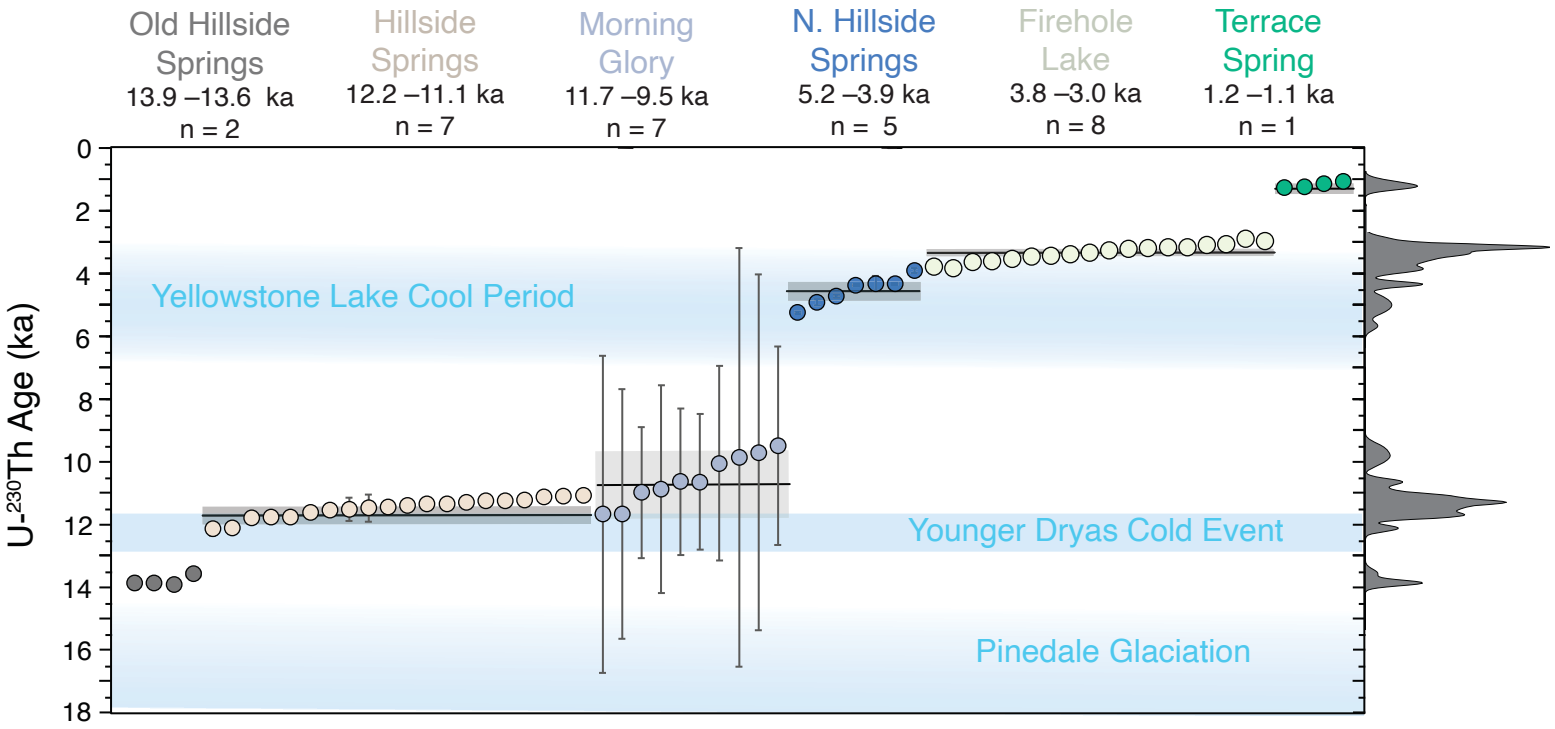
Old Hillside Springs
13.9 –13.6 ka
n = 2
Hillside Springs
12.2 –11.1 ka
n = 7
Morning Glory
11.7 –9.5 ka
n = 7
N. Hillside Springs
5.2 –3.9 ka
n = 5
Firehole Lake
3.8 –3.0 ka
n = 8
Terrace Spring
1.2 –1.1 ka
n = 1
Yellowstone Lake Cool Period
Younger Dryas Cold Event
Pinedale Glaciation
U-230Th Age (ka)
0
2
4
6
8
10
12
14
16
18

Figure 4

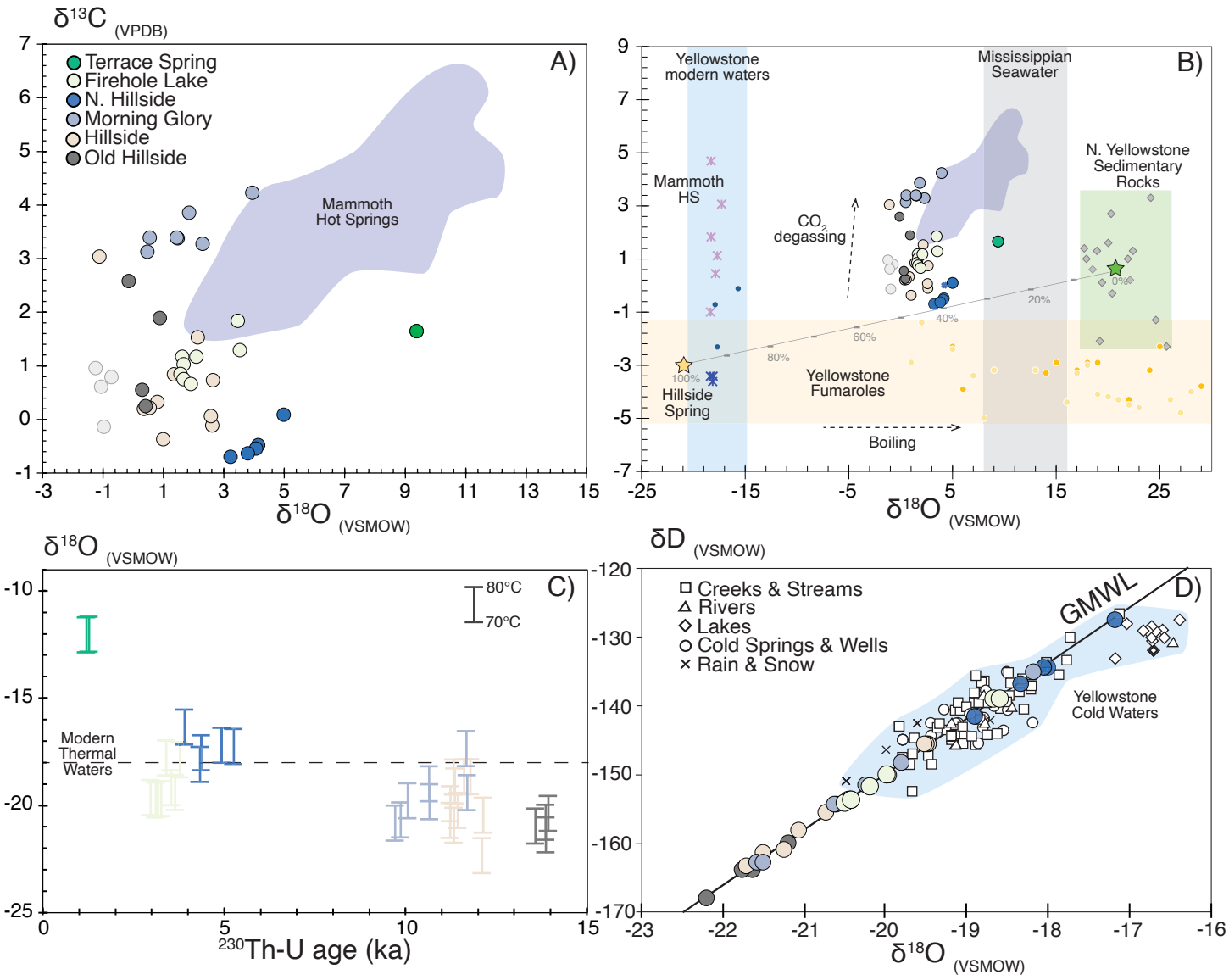
δ13C (VPDB)
A)
Terrace Spring
Firehole Lake
N. Hillside
Morning Glory
Hillside
Old Hillside
Mammoth Hot Springs
δ18O (VSMOW)
B)
Yellowstone modern waters
Mississippian Seawater
Mammoth HS
CO2 degassing
N. Yellowstone Sedimentary Rocks
0%
20%
40%
60%
80%
100%
Hillside Spring
Yellowstone Fumaroles
Boiling
δ18O (VSMOW)
δ18O (VSMOW)
C)
80°C
70°C
Modern Thermal Waters
230Th-U age (ka)
δD (VSMOW)
D)
Creeks & Streams
Rivers
Lakes
Cold Springs & Wells
Rain & Snow
GMWL
Yellowstone Cold Waters
δ18O (VSMOW)

Figure 5

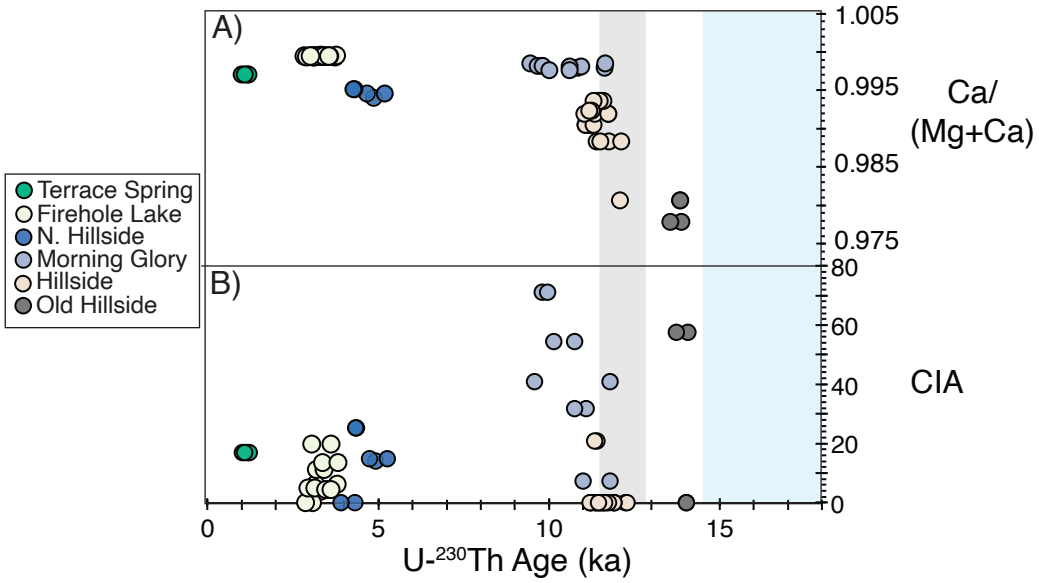
A)
B)
Terrace Spring
Firehole Lake
N. Hillside
Morning Glory
Hillside
Old Hillside
1.005
0.995
0.985
0.975
Ca/
(Mg+Ca)
80
60
40
20
0
CIA
0
5
10
15
U-230Th Age (ka)

Figure 6

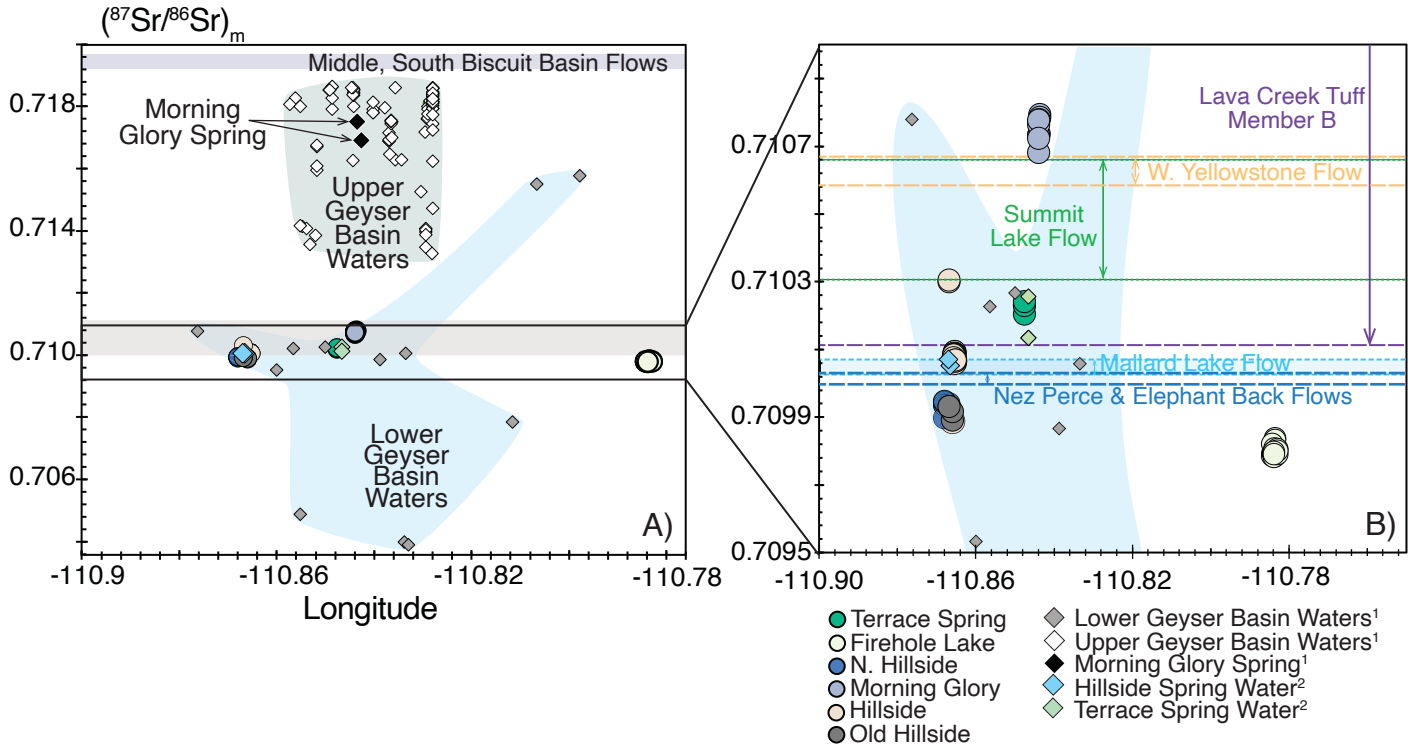
$(^{87}Sr/^{86}Sr)_m$
Middle, South Biscuit Basin Flows
Morning Glory Spring
Upper Geyser Basin Waters
Lower Geyser Basin Waters
A)
0.718
0.714
0.710
0.706
-110.9
-110.86
-110.82
-110.78
Longitude
Lava Creek Tuff Member B
W. Yellowstone Flow
Summit Lake Flow
Mallard Lake Flow
Nez Perce & Elephant Back Flows
B)
0.7107
0.7103
0.7099
0.7095
-110.90
-110.86
-110.82
-110.78
Terrace Spring
Firehole Lake
N. Hillside
Morning Glory
Hillside
Old Hillside
Lower Geyser Basin Waters[1]
Upper Geyser Basin Waters[1]
Morning Glory Spring[1]
Hillside Spring Water[2]
Terrace Spring Water[2]

Figure 7

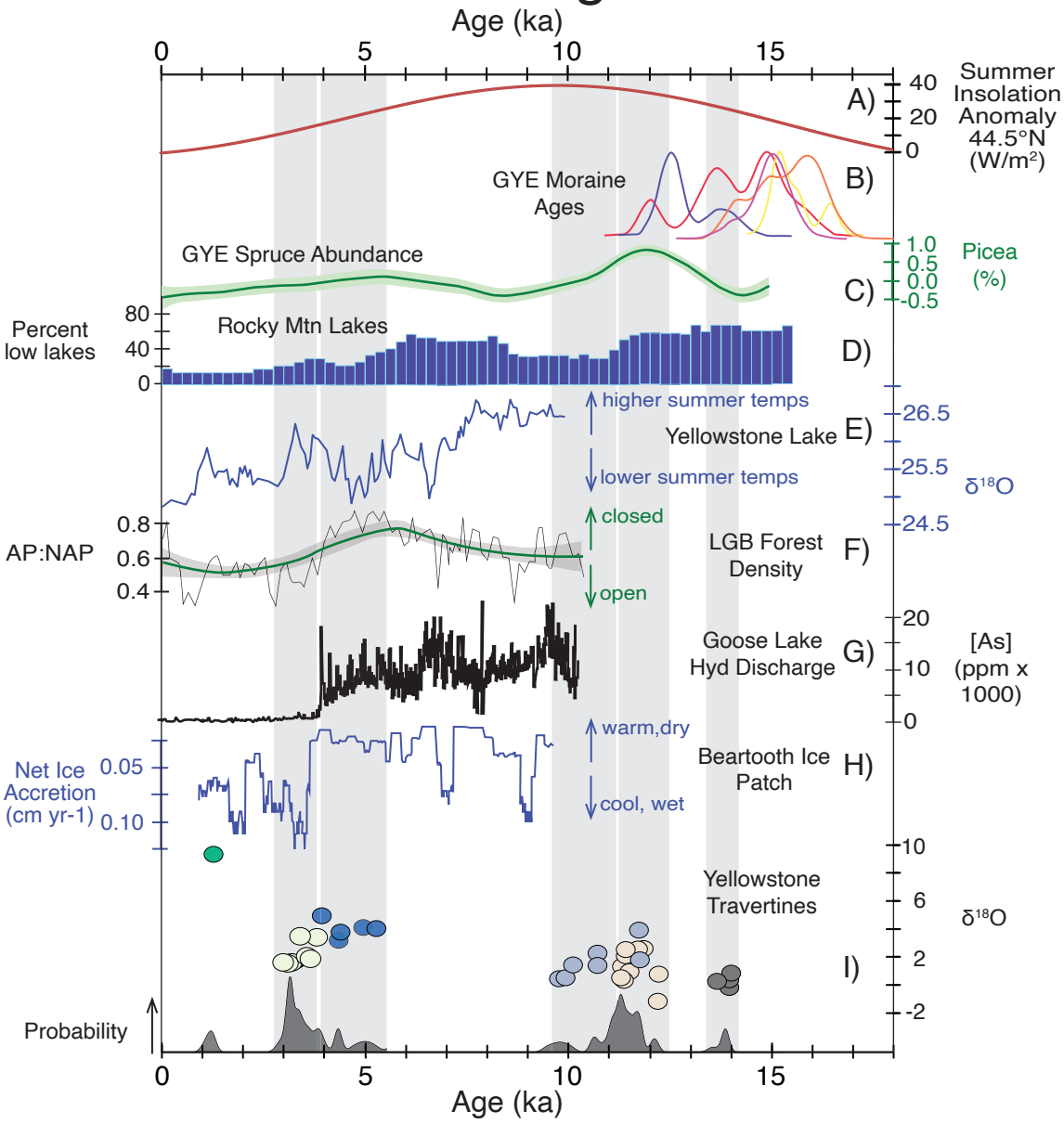
Age (ka)
0
5
10
15
A)
Summer Insolation Anomaly 44.5°N (W/m²)
40
20
0
GYE Moraine Ages
B)
GYE Spruce Abundance
C)
1.0
0.5
0.0
-0.5
Picea (%)
Percent low lakes
80
40
0
Rocky Mtn Lakes
D)
higher summer temps
lower summer temps
Yellowstone Lake
E)
26.5
25.5
24.5
δ18O
AP:NAP
0.8
0.6
0.4
closed
open
LGB Forest Density
F)
Goose Lake Hyd Discharge
G)
20
10
0
[As] (ppm x 1000)
warm,dry
cool, wet
Beartooth Ice Patch
H)
Net Ice Accretion (cm yr-1)
0.05
0.10
Yellowstone Travertines
10
6
2
-2
δ18O
I)
Probability
0
5
10
15
Age (ka)

Table 1. Calcuated CO_2 flux from intra-caldera travertine volume

Location	Surface area of travertine outcrop (m^2)	Estimated thickness of deposit (m)	Minimum age (ka)	Maximum age (ka)	Volume (m^3)	Metric tons CO_2*	CO_2 flux (tons/year)	CO_2 flux (tons/day)
Hillside Springs	138,797	4	11.1	13.9	$5.5x10^5$	$5.8x10^5$	$2.1x10^2$	0.6
N. Hillside Spring	310	3	3.9	5.2	$7.8x10^2$	$8.0x10^2$	1	0.0
Morning Glory	1,973	1	9.5	11.7	$1.9x10^3$	$2.0x10^3$	1	0.0
Firehole Lake	24,710	3	3.0	3.8	$7.5x10^3$	$7.8x10^3$	10	0.0
Terrace Spring	298,110	1	1.1	1.2	$1.5x10^5$	$1.5x10^5$	$1.5x10^3$	4.2#
TOTAL	463,900	11	-	-	$7.1x10^5$	$7.4x10^5$	$1.8x10^3$	5

*We assume the density of calcite is 2.7 g/cm^3, travertine porosity is 10%, and the mineralogy is 97% $CaCO_3$ for a bulk density of 2.43 g/cm^3. The flux of CO_2 is calculated according to the equation $moles_{CO} = moles_{CaCO_3} = (V \times \rho b \times f)/M$ where V is volume, ρb is the bulk density, f is the fraction of $CaCO_3$ in travertine, and M is the molar mass of $CaCO_3$ (Mancini et al., 2019).

#The age of this deposit is not well constrained and this value therefore has a high level of uncertainty. If the deposit formed over a greater time span, the calculated flux would be smaller.